Appendix O. Collision Consequence

O.1 Introduction

It is common in conjunction assessment circles to speak of "collision risk metrics" such as the Probability of Collision (Pc), but in fact, calling such parameters risk metrics is a misnomer. As was first laid out formally in the literature by Kaplan and Garrick (1981) and has been adapted and reinforced by NASA's own project risk assessment paradigms, risk is actually the combination of the likelihood of a detrimental event and the consequence if such an event should come to pass. Conjunction risk assessment metrics such as the Pc are simply measures of collision likelihood, which is only part of the overall risk assessment. Because conjunction assessment practice arose originally from individual missions whose focus was to protect their own spacecraft, it seemed unnecessary to add any considerations beyond collision likelihood. The loss of the mission's spacecraft was considered a catastrophic event to be avoided at all costs, so all that needed to be evaluated was the likelihood of a collision, which if it took place was presumed to be fatal to the satellite's operation and the mission.

When the conjunction assessment risk analysis for groups of satellites or an entire agency or nation is considered, however, the problem broadens. There is certainly the desire to see individual missions protected from catastrophic termination. The particular urgency of protecting any given spacecraft from premature end-of-mission life is a product of a number of factors such as the degree to which mission objectives have been met, the age of the satellite, and the functional redundancy within a constellation. Because the individual mission has the best sense of these considerations, they are in the best position to assess the consequences of potential spacecraft loss. However, there is a second parallel consideration, which is the preservation of orbital corridors from debris pollution to ensure their utility for future missions, both by the United States and all space-faring nations. The NASA Orbital Debris Program Office (ODPO) has for some years been the NASA project chartered with this concern. They have outlined spacecraft design and disposal recommendations to mitigate orbital debris production, but there has not yet been an effort to establish clear requirements for debris minimization through on-orbit conjunction assessment activities during mission lifetimes. One of the purposes of the present document is to lay out best practices for conjunction assessment operations that promote debris minimization. To reduce the production of debris, one must not only consider the likelihood of any given collision between a NASA primary satellite and other space objects but also evaluate the amount of debris that such a conjunction, should it result in a collision, may engender.

O.2 Debris Production Determination Methodology

It is very much the case that different types of satellite collisions can produce substantially different amounts of debris. The ODPO has studied this phenomenon in some depth through staged collisions of satellites with simulated debris objects in vacuum chambers and established relationships among conjunction parameters and the number and size of the resultant debris objects (Johnson et al. 2001). The basic distinction is between catastrophic collisions, in which both the primary and secondary object are fully fragmented and thus generate large amounts of

debris, and non-catastrophic collisions in which the smaller/lighter satellite is fully fragmented but the larger/heavier satellite only cratered, generating much smaller amounts of debris. The catastrophic/non-catastrophic distinction is governed by the following relationship, based on the relative kinetic energy of the encounter:

$$\varepsilon = \frac{\min(M_1, M_2)}{\max(M_1, M_2)} \left(\frac{V_{rel}^2}{2} \right) \tag{O-1}$$

in which V_{rel} is the relative velocity between the two satellites, M_1 is the mass of the primary satellite, and M_2 is the mass of the secondary satellite. When the relative kinetic energy exceeds 40,000 Joules per kilogram, ε_*, the collision is expected to be catastrophic and produce much larger amounts of debris. The ODPO has further developed a relationship that estimates the number of debris pieces greater than a specified size that the collision will generate:

$$F_{EV}(M_1, M_2) = \begin{cases} 0.1(V_{rel} \min(M_1, M_2))^{0.75} L_c^{-1.71} & \text{if } \varepsilon \leq \varepsilon_* \text{ (noncatastrophic)} \\ 0.1(M_1 + M_2)^{0.75} L_c^{-1.71} & \text{if } \varepsilon > \varepsilon_* \text{ (catastrophic)} \end{cases} \tag{O-2}$$

in which L_c is the characteristic length (size) above which one wishes to determine the number of debris pieces. According to Lechtenberg and Hejduk (2019) and Lechtenberg (2019a), "trackable" fragments are those with characteristic lengths exceeding a cutoff of $L_c = 0.05$ m. If the collision is catastrophic, the number of fragments is determined by the sum of the two satellites' masses; if it is non-catastrophic, the equation uses the product of the mass of the lighter satellite and the conjunction's relative velocity.

These relationships conform to first-order intuition regarding expected relative levels of debris production. Any schoolboy who has played with dirt clods can testify that a greater relative velocity between two conjuncting dirt clods will produce greater fragmentation. Furthermore, if the masses of the heavier and lighter object differ substantially, which probably also means that their relative sizes differ as well, one can imagine the (much) smaller object simply passing through (cratering) the larger one and, while itself fragmenting, leaving the larger object essentially intact. This full versus partial fragmentation division introduces a discontinuity in the debris production relationship (as a function of relative mass and relative velocity), and the entire dynamic, illustrated by Figure O-1, shows the extremely broad range of debris production outcomes—from very few debris pieces to thousands—all of which represent real possibilities for satellite conjunctions because the full range of secondary object mass values and relative velocities shown in the figure are frequently encountered in practice.

To assess fragmentation risks a collision presents to the orbital environment, Hall and Baars (2022) introduced a "fragmentation probability" metric that measures a conjunction's probability of producing more than a threshold number of trackable fragments, F, given by:

$$\bar{P}_F = \mathbb{E}[P_F(R_1, R_2, M_1, M_2)] \approx \mathbb{E}[P_c(R_1 + R_2) \times U(F_{EV}(M_1, M_2) - F)] \tag{O-3}$$

where R_1 and R_2 are the primary and secondary object's hard-body radii (HBR), respectively, $U(-)$ is the unit step function, and $\mathbb{E}[-]$ is the expectation value operator, which indicates the expected results by averaging over all relevant random variables.

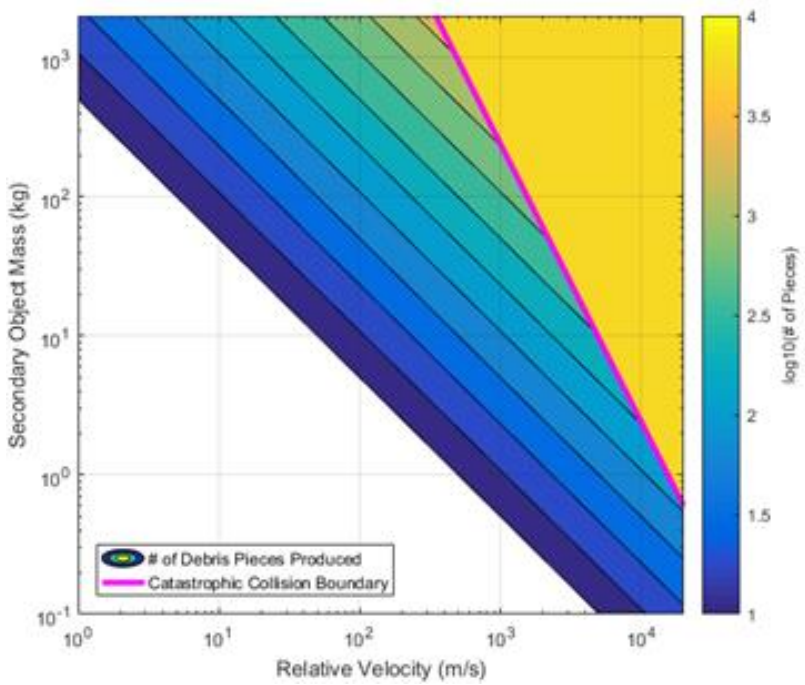

Figure O-1 Range of Debris Production Possibilities[19]

Since the debris production potential can vary so greatly among different conjunctions, it makes sense that conjunction remediation requirements should take cognizance of this parameter, presuming of course that it can be estimated from available conjunction information. The conjunction relative velocity is easy to calculate and is in fact provided directly as part of the CDM, and the HBR and mass of the primary object are known by the satellite O/O. The HBR and mass of the secondary object, however, are more elusive; in the great majority of conjunctions, this object is a debris object for which there is no *a priori* information. One must therefore look to estimation processes to estimate this object's HBR and mass.

In formulating a HBR and mass estimation methodology, an approach is desired that is informed by and accounts for associated uncertainties in the estimate. If conjunction mitigation requirements are to be somewhat relaxed for low-debris-potential conjunctions, it is important to err on the side of debris quantity overestimation to guarantee that all situations in which this relaxed threshold may be applied are truly warranted. In nearly all practical cases, larger secondary object HBR and mass values will result in larger produced debris counts. A conservative approach requires ensuring, to a desired degree, that the estimation process overestimate rather than underestimate the HBR and mass of the secondary object. Such an orientation can be tuned and verified by attempting to estimate the HBR and mass of small objects with known HBR and mass values such as microsats.

[19] From Hejduk et al. 2019.

O.3 Estimating the Sizes of Unknown Objects

Stokely *et al* (2006) describe the NASA size estimation model (SEM), which provides a semi-empirical method to convert radar cross-section (RCS) measurements for an unknown satellite into a statistical ensemble of estimates for the "characteristic length" of the object. Notably, this characteristic length is not equivalent to the hard-body radius, but instead represents the average of the largest dimensions of an object measured along three orthogonal axes, which corresponds to the diameter for spherical objects. Applying the SEM to the n^{th} RCS measurement available for the j^{th} satellite yields:

$$D_{j,n} = \begin{cases} \lambda_{j,n}\sqrt{4z/\pi} & z > 5 \\ \lambda_{j,n}\sqrt[6]{4z/(9\pi^5)} & z < 0.03 \\ \lambda_{j,n}\, g_{SEM}(z) & otherwise \end{cases} \quad \text{(O-4)}$$

with $D_{j,n}$ denoting the characteristic length (m) corresponding to the RCS measurement, $\lambda_{j,n}$ the radar wavelength (m), and $z = Y_{j,n}/\lambda_{j,n}^2$, with $Y_{j,n}$ representing the measured RCS value (m^2). Stokley *et al* (2006) provide an interpolation table for the function $g_{SEM}(z)$. Notably, the NASA SEM provides no direct means to estimate the error or uncertainty of RCS-based characteristic length estimates. This can be especially problematic if only one representative (e.g., median) RCS value is available per satellite. As described in Hall and Baars (2022), numerous RCS measurements are used per satellite over extended time periods (e.g., ~1,000 RCS measurements acquired over ~2 years) to analyze the resulting characteristic length distributions to estimate both the unknown hard-body radii and the associated uncertainties.

To start the HBR estimation process, Space Fence RCS data are collected for the two years prior to the calibration epoch date. The analysis is restricted to objects with twenty or more well calibrated and quality-curated Space Fence system RCS measurements, as described in detail by Baars and Hall (2022). Next, the NASA SEM is used to estimate RCS-based characteristic length estimates for each satellite, which typically have considerable point-to-point variability or scatter. Sources of this scatter include the object's aspect-dependent radar reflection properties and projected area (which vary in time due to rotation and changing observational geometry), as well as RCS measurement noise (which is often relatively minor). Empirical cumulative distribution functions (CDFs) and probability density functions (PDFs) are generated from these data.

Using the empirical PDF approximation, the mean characteristic length for the j^{th} satellite is:

$$\bar{D}_j \approx \frac{1}{N_j^{RCS}} \sum_{n=1}^{N_j^{RCS}} D_{j,n} \quad \text{(O-5)}$$

The corresponding variance is:

$$\sigma_{\bar{D}_j}^2 \approx \frac{1}{N_j^{RCS}} \sum_{n=1}^{N_j^{RCS}} \left(D_{j,n} - \bar{D}_j\right)^2 \quad \text{(O-6)}$$

with N_j^{RCS} indicating the number of RCS measurements for the j^{th} satellite. Since the variable radar reflection properties of a satellite causes some of the variation of the $D_{j,n}$ values, the empirical PDF approximation tends to overestimate the variance of the object's actual characteristic size distribution.

If the SEM were free of any estimation inaccuracies and the RCS measurements were free of any measurement noise, then the relationship between the circumscribing HBR and the characteristic length for idealized spherical objects would be relatively simple: $R_j = D_j/2$. To quantify the bias and uncertainty for noisy measurements of actual non-spherical objects, a calibration factor is introduced into this relationship, expressed in either linear or logarithmic form as follows:

$$R_j = \Omega_j(D_j/2) = e^{\omega_j}(D_j/2) \tag{O-7}$$

The formulation assumes that the calibration factors Ω_j and $\omega_j = \log_e(\Omega_j) = \ln(\Omega_j)$ are time invariant, but that they vary from satellite to satellite.

Hall and Baars (2022) uses a set of relatively small calibration satellites that all have convex cuboid shapes. Specifically, the calibration analysis employs sizes obtained from the *Database and Information System Characterising Objects in Space* (DISCOS), which tabulates the bounding dimensions and general shape descriptions of a large number of known satellites.[20] The calibration analysis is restricted to satellites labeled as "box" shaped in the DISCOS database, and that have no tabulated additional panels or attachments. The circumscribing HBR for a box-shaped satellite with sides of length $\mathcal{L}_j$, width $\mathcal{W}_j$ and height $\mathcal{H}_j$, is given by:

$$R_j^K = \frac{1}{2}\sqrt{\mathcal{L}_j^2 + \mathcal{W}_j^2 + \mathcal{H}_j^2} \tag{O-8}$$

The calibration analysis is also restricted to DISCOS satellites with $R_j^K \leq 0.35$ m, which are comparably small to the typical unknown debris objects involved in CARA conjunctions.

Space Fence observations collected in the two years preceding a calibration epoch date provide usable RCS measurements of box-shaped satellites tabulated in the DISCOS database.[21] Each of these provides an independent (albeit noisy) measurement of the logarithmic calibration factor:

$$\omega_j = \ln\left(2R_j^K/\bar{D}_j\right) \tag{O-9}$$

Sivia and Skilling (2006) present a Bayesian analysis approach that can be used to estimate the mean logarithmic calibration factor from the set $\{\omega_j, j = 1 \ldots J\}$, with J equal to the number of selected calibration satellites from the DISCOS database which also have Space Fence RCS data. The method assumes that satellite-to-satellite variations in the ω_j values are Gaussian-distributed, and applies an uninformed-prior Bayesian analysis method to derive the maximum posterior estimates for the mean calibration factor and variance:

[20] From Flohrer *et al* (2013) and Mclean *et al* (2017).
[21] https://discosweb.esoc.esa.int/

$$\bar{\omega} = \frac{1}{J}\sum_{j=1}^{J}\omega_j \quad \text{and} \quad \sigma_\omega^2 = \frac{1}{J-1}\sum_{j=1}^{J}\left[\omega_j - \bar{\omega}\right]^2 \tag{O-10}$$

As an example, for the calibration epoch date of 2022-01-15, sufficient RCS data are available for $J = 586$ of the DISCOS box-shaped satellites. The calibration analysis yields $\bar{\omega} = 0.319$ and $\sigma_\omega = 0.507$. The estimate for σ_ω indicates significant satellite-to-satellite variation in the calibration factors.

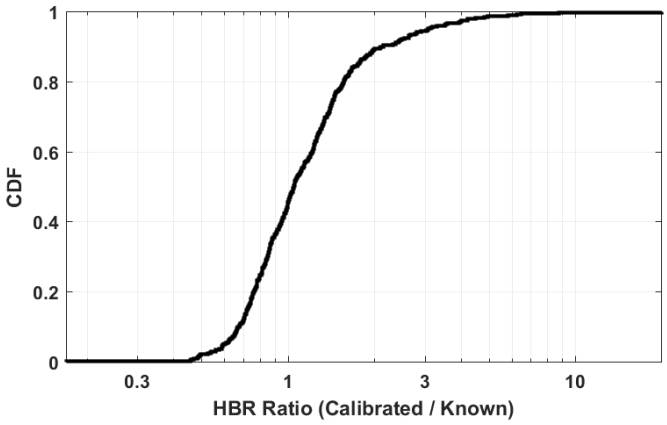

Figure O-2 CDF of the Ratio of Calibrated HBR Values to Known HBR Values for 586 Satellites[22]

Figure O-2 compares the empirical CDF of the ratio of calibrated RCS-based HBR values to the known values for the 586 satellites. The CDF indicates that, among this population, calibration uncertainties limit the 95% confidence accuracy range of the HBR estimation process to within a factor of 2.4 for potential underestimations, and to within a factor of 3.1 for potential overestimations.

O.4 Estimating the Masses of Unknown Objects

Several approaches may be used to estimate the mass of an unknown object, the first involves the use of the orbit determination-based ballistic coefficient (BC) estimate while the second uses the orbit determination-based solar radiation pressure coefficient (SRPC) estimate. For satellites that experience measurable atmospheric drag orbital perturbations, the BC estimation method is preferred. However, for satellites with a perigee height above 450 km in altitude, the SRPC mass estimates are somewhat more accurate.

O.4.1. RCS + Ballistic Coefficient Method

Combining RCS-based size estimates and orbit determination -based BC estimates provides a means to estimate the masses of LEO satellites that experience measurable atmospheric drag.

[22] From Hall and Baars (2022)

This "RCS+BC" mass estimation method approximates the characteristic mass of a LEO satellite using an expression formulated previously[23]:

$$\mathcal{M}_{D,j} = A_j B_j C_{D,j} \approx (\pi D_j^2/4) B_j C_{D,j} \tag{O-11}$$

In this expression, $\mathcal{M}_{D,j}$ indicates the mass that characterizes the atmospheric drag experienced by the j^{th} satellite, which is proportional to the product of the projected area, A_j, the inverse ballistic coefficient, B_j, and the drag coefficient, $C_{D,j}$. The analysis uses RCS-based characteristic projected areas to estimate satellite cross sectional areas projected normal to the local atmospheric flow, $A_j \approx (\pi D_j^2/4)$, which is a rough approximation, especially for highly elongated or flattened objects. As before, a positive scalar calibration factor, Ψ_j, is introduced to equation O-11 to quantify the bias and uncertainty of the RCS+BC mass estimation process:

$$M_j \approx \Psi_j \mathcal{M}_{D,j} = e^{\psi_j}\left[(\pi D_j^2/4) B_j C_{D,j}\right] \tag{O-12}$$

with M_j indicating the calibrated mass of the satellite, Ψ_j the linear calibration factor, and ψ_j the logarithmic calibration factor. Again, the analysis assumes these calibration factors are time invariant, but do vary from satellite to satellite. Applying equation O-12 to the j^{th} calibration satellite yields:

$$M_j^K = e^{\psi_j}\mathbb{E}\left[\mathcal{M}_j\right] \approx e^{\psi_j}\left[\bar{A}_j \bar{B}_j \bar{C}_{D,j}\right] \tag{O-13}$$

This approximation neglects correlations between the quantities D_j, B_j, and $C_{D,j}$. In order to use equation O-13, the mean projected area, inverse ballistic coefficient, and drag coefficient will need to be calculated for each satellite.

The mean projected area is approximated from the mean characteristic length and associated variance:

$$\bar{A}_j = \mathbb{E}\left[A_j\right] \approx \pi\left(\bar{D}_j^2 + \sigma_{D_j}^2\right)/4 \tag{O-14}$$

The formulation approximates the inverse ballistic coefficient PDF, by first empirically estimating the ballistic coefficient mean and variance parameters, and then assuming a lognormal distribution of the form:

$$\rho\left(B_j\right) \approx \frac{\mathcal{N}\left(\ln\left(B_j\right), \bar{b}_j, \sigma_{b_j}^2\right)}{B_j} \tag{O-15}$$

with $\sigma_{b_j}^2 = \ln\left(1 + \sigma_{B_j}^2/\bar{B}_j^2\right)$ and $\bar{b}_j = \ln\left(\bar{B}_j\right) - \sigma_{b_j}^2/2$. (Note: Sampling this PDF, as will later be required for Monte Carlo estimations, cannot produce negative B_j values, which are physically unrealistic for satellites that experience measurable levels of atmospheric drag. This unrealism is why this analysis does not assume a PDF of the form $\mathcal{N}\left(B_j, \bar{B}_j, \sigma_{B_j}^2\right)$, which can potentially produce negative sampled values.) The mean and variance of the inverse ballistic coefficient, $\bar{B}_j$

[23] From Lechtenberg 2019a.

and $\sigma_{B_j}^2$, respectively, are estimated empirically by combining a set of orbit determination solutions accumulated over the six months prior to the calibration epoch date. Specifically, the analysis uses a series of orbit determination solutions separated by one week or more in time that each represent an orbit determination solution for the j^{th} satellite. The corresponding ballistic coefficients, $\{(\beta_{j,m}, \Delta\beta_{j,m}), m = 1 \ldots N_j^{VCM}\}$, typically number $N_j^{VCM} \approx 25$ for most satellites. The ballistic coefficients, $\beta_{j,m}$, and associated 1-sigma orbit determination estimation uncertainties, $\Delta\beta_{j,m}$, are then combined using a weighted averaging scheme. The first step in the process is to calculate the inverse ballistic coefficient and uncertainty for the m^{th} Vector Covariance Message (VCM) available for the j^{th} satellite:

$$\mathrm{B}_{j,m} = 1/\beta_{j,m} \quad \text{and} \quad \Delta\mathrm{B}_{j,m} = \Delta\beta_{j,m}/\beta_{j,m}^2 \tag{O-16}$$

The next step calculates the weighted average:

$$\bar{B}_j = \frac{1}{W_j} \sum_{m=1}^{N_j^{VCM}} W_{j,m} B_{j,m} \tag{O-17}$$

with $W_{j,m} = \left(\Delta\mathrm{B}_{j,m}\right)^{-2}$ and $W_j = \sum_m W_{j,m}$. The analysis estimates the variance using a hybrid scheme as follows:

$$\sigma_{\mathrm{B}_j}^2 = \max\left(W_j^{-1}, V_j\right) \tag{O-18}$$

with

$$V_j = W_j^{-1} \left[\frac{N_j^{VCM}}{N_j^{VCM} - 1} \sum_{m=1}^{N_j^{VCM}} W_{j,m} \left(\mathrm{B}_{j,m} - \overline{\mathrm{B}}_j\right)^2 \right]^{1/2} \tag{O-19}$$

This scheme conservatively uses the larger of the variances estimated using two methods: the first assumes statistical independence of the $\mathrm{B}_{j,m}$ values, yielding variance equal to W_j^{-1}; the second accounts for the observed scatter of the $\mathrm{B}_{j,m}$ values, yielding the empirically estimated variance equal to V_j. In the rare cases when only one orbit determination solution is available for an object, the analysis uses $\sigma_{B_j}^2 = W_j^{-1} = \left(\Delta\mathrm{B}_{j,m}\right)^2$ for the variance.

Finally, the analysis approximates the PDF for the satellite drag coefficients $C_{D,j}$ using a uniform distribution spanning a fixed, bounded range:

$$\rho\left(C_{D,j}\right) \approx \begin{cases} \left(C_{D,max} - C_{D,min}\right)^{-1} & \text{if } C_{D,min} \le C_{D,j} \le C_{D,max} \\ 0 & \text{otherwise} \end{cases} \tag{O-20}$$

This study uses the bounds $C_{D,min} = 2.1$ and $C_{D,max} = 2.9$ for all objects, based on the range of drag coefficients presented in previous analyses.[24] The uniform PDF yields a mean of $\bar{C}_{D,j} = (C_{D,max} + C_{D,min})/2 = 2.5$, and variance $\sigma^2_{C_{D,j}} = \left(C_{D,max} - C_{D,min}\right)^2/12 = 0.053$ (i.e. $\sigma_{C_{D,j}} = 0.23$).

The mass calibration process uses box-shaped DISCOS satellites, as described previously for the HBR calibration process. Each calibration satellite that has sufficient RCS data and VCM BC estimates provides an independent (albeit noisy) measurement of the logarithmic calibration factor, $\psi_j = \ln\left[M_j^K/(\bar{A}_j\bar{B}_j\bar{C}_{D,j})\right]$, yielding combined estimates of:

$$\bar{\psi} = \frac{1}{J}\sum_{j=1}^{J}\psi_j \quad and \quad \sigma^2_{\psi} = \frac{1}{J-1}\sum_{j=1}^{J}\left[\psi_j - \bar{\psi}\right]^2 \tag{O-21}$$

derived by applying the same Bayesian method used for the HBR calibration process.

For the calibration epoch date of 2022-01-15, sufficient RCS data and VCM BC estimates are available for $J = 554$ of the DISCOS box-shaped satellites. The calibration analysis yields $\bar{\psi} = -0.159$ and $\sigma_{\psi} = 0.959$. The estimated σ_{ψ} value indicates significant satellite-to-satellite variation among the calibration satellites.

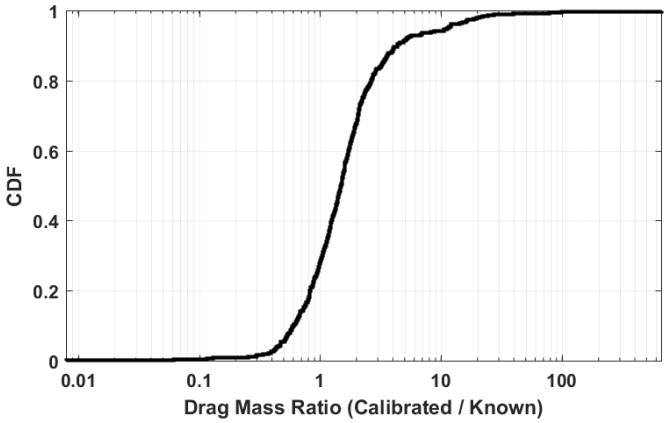

Figure O-3 CDF of the Ratio of Calibrated RCS+BC Mass Estimates to Known Masses for 554 Satellites[25]

Figure O-3 compares the empirical CDF of the ratio of calibrated mass estimates to the known values for the 554 satellites. The CDF indicates that, among this population, calibration uncertainties limit the 95% confidence accuracy range of the RCS+BC mass estimation process to within a factor of 4.1 for potential mass underestimations, and to within a factor of 10.4 for potential mass overestimations.

[24] From Lechtenberg and Hejduk (2019) and Lechtenberg (2019a).
[25] From Hall and Baars (2022)

O.4.2. RCS + Solar Radiation Pressure Coefficient Method

Combining RCS-based size estimates and orbit determination-based solar radiation pressure coefficient estimates provides a means to estimate the masses of satellites that experience measurable solar radiation pressure (SRP) perturbations. This "RCS+SRPC" mass estimation analysis approximates the characteristic mass of a LEO satellite using an expression similar in form to that used for RCS+BC based mass estimation given by equation O-11:

$$\mathcal{M}_{R,j} \approx \left(\pi D_j^2/4\right) G_j C_{R,j} \tag{O-22}$$

In this expression, $\mathcal{M}_{R,j}$ indicates the mass that characterizes SRP perturbations experienced by the j^{th} satellite, which is proportional to the product of three quantities: the area projected towards the incident sunlight (again approximated using $\pi D_j^2/4$), the inverse solar radiation pressure coefficient, G_j, and the reflectivity coefficient, $C_{R,j}$. See Vallado (2001) for more details on orbital SRP perturbations. As before, this study introduces a positive scalar calibration factor, Θ_j, into equation O-22 to quantify the bias and uncertainty of the RCS+SRPC mass estimation process:

$$M_j \approx \Theta_j \mathcal{M}_{R,j} = e^{\theta j}\left[\left(\pi D_j^2/4\right) G_j C_{R,j}\right] \tag{O-23}$$

with M_j indicating the calibrated mass of the satellite, Θ_j the linear calibration factor, and θ_j the logarithmic calibration factor. The process of estimating the calibration factors for the RCS+SRPC mass estimation process uses the same exact analysis steps as outlined in the previous section for the RCS+BC mass estimation process but substitutes the orbit determination-based inverse solar radiation pressure coefficient, G_j, for the inverse ballistic coefficient, B_j, and also substitutes the reflectivity coefficient, $C_{R,j}$, for the drag coefficient, $C_{D,j}$. The analysis assumes a uniform PDF with bounds $C_{R,min} = 1$ and $C_{R,max} = 1.4$ for all satellites, which yields a mean of $\bar{C}_{R,j} = 1.2$, and variance $\sigma^2_{C_{R,j}} = 0.013$ (i.e., $\sigma_{C_{R,j}} = 0.12$). The lower bound of $C_{R,min} = 1$ corresponds to that expected for dark bodies (i.e., that have negligible overall reflectance) of any shape. The upper bound of $C_{R,max} = 1.4$ represents the theoretical value for a Lambertian sphere with 90% reflectance,[26] and is assumed to provide a reasonable upper limit for unknown secondary objects.

The analysis restricts RCS+SRPC mass estimation to satellites with perigee altitudes above 450 km altitude to ensure that imperfectly modeled atmospheric drag perturbations do not bias the solar radiation pressure coefficients estimated in the orbit determination analysis, which has been observed to occur for LEO satellites at lower altitudes. For the calibration epoch date of 2022-01-15, sufficient RCS data and VCM SRPC estimates are available for $J = 303$ of the DISCOS cuboid satellites with perigees above 450 km altitude. The calibration analysis yields $\bar{\theta} = 0.173$ and $\sigma_\theta = 0.884$.

[26] From Li *et al* (2018).

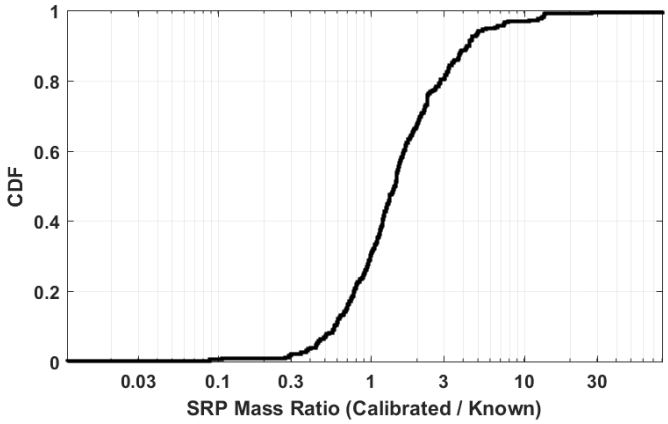

Figure O-4 CDF of the Ratio of Calibrated RCS+SRPC Mass Estimates to Known Masses for 303 Satellites[27]

Figure O-4 compares the empirical CDF of the ratio of calibrated mass estimates to the known values for the 303 satellites. The CDF indicates that, among this population, calibration uncertainties limit the 95% confidence accuracy range of the RCS+SRPC mass estimation process to within a factor of 3.8 for potential mass underestimations, and to within a factor of 8.4 for potential mass overestimations. This means that, for satellites with perigee altitudes above 450 km, the RCS+SRPC method provides somewhat more accurate mass estimates than the RCS+BC estimation method, although both methods provide rough mass estimates overall.

O.5. The Probability of Exceeding a Threshold Number of Trackable Fragments

Recall equation O-3 that defines a fragmentation probability metric, which is calculated using an expectation value to determine the probability that a conjunction will generate more than a threshold number of trackable fragments. For known-on-unknown conjunctions, calculating this expectation value represents integrating over a set of five random variables that account for the size and mass estimation uncertainties of the secondary object. Specifically, for the RCS+BC mass estimation method, these five random variables are $\{D_2, \omega_2, \psi_2, B_2, C_{D,2}\}$; for RCS+SRPC mass estimation they are $\{D_2, \omega_2, \theta_2, G_2, C_{R,2}\}$. Correspondingly, unknown-on-unknown collisions require integrations over ten random variables associated with both objects. In other words, estimating the statistically expected fragmentation probability, $\bar{P}_F$, entails evaluating either a 5-D or 10-D integral. The integrand function of these multi-dimensional integrals contains the product of the conjunction's collision probability, $P_c(R_1 + R_2)$, and the binary probability that the number of fragments, $F_{EV}(M_1, M_2)$, exceeds the threshold value, F. Both of these functions are non-linear, and the latter possesses discontinuities. The Monte Carlo method provides and efficient and straightforward means of computing such multi-dimensional integrals.

[27] From Hall and Baars (2022)

Focusing on the known-on-unknown collision case for the RCS+BC mass estimation method, the five random variables are computed as follows:

1. D_2 is modeled as a normally distributed variable using the mean and variance defined in equations O-5 and O-6.
2. ω_2 is modeled as a normally distributed variable using the mean and variance defined in equation O-10.
3. ψ_2 is modeled as a normally distributed variable using the mean and variance defined in equation O-21.
4. B_2 is modeled as a normally distributed variable in logarithmic space using the mean and variance defined directly below equation O-15.
5. $C_{D,2}$ is modeled as a uniformly distributed variable with $C_{D,min} = 2.1$ and $C_{D,max} = 2.9$.

The RCS+SRPC mass estimation method uses the same computations for D_2 and ω_2. For the remaining variables, ψ_2 is replaced with θ_2, B_2 is replaced with G_2, and $C_{D,2}$ is replaced with $C_{R,2}$ (along with the associated $C_{R,min}$ and $C_{R,max}$ values).

In the Monte Carlo method these random variables are used to generate a set of R_2 and M_2 values for a number of Monte Carlo trials, N_{MC}. The fragmentation probability is then estimated as:

$$\bar{P}_F \approx \frac{1}{N_{MC}} \sum_{n=1}^{N_{MC}} \left[P_c\left(R_1 + R_{2,n}\right) \times U\left(F_{EV}\left(M_1, M_{2,n}\right) - F\right) \right] \tag{O-24}$$

For $F = 0$, it is straightforward to show that $\bar{P}_F = \bar{P}_c$. More generally, a conjunction's fragmentation probability cannot exceed the collision probability, $\bar{P}_F \leq \bar{P}_c$. For groups like CARA that use the collision probability to assess close approach risks, this inequality property makes $\bar{P}_F$ a convenient choice to assess environmental risks, for two reasons. First, if the screening process indicates that $\bar{P}_c$ is less than a negligibly small green-level cutoff (i.e., 10^{-10}), then $\bar{P}_F$ also must be less than that cutoff. Second, the inequality implies that all conjunctions that represent red-level environmental risks (i.e., those with $\bar{P}_F \geq 10^{-4}$) are naturally contained within the set of conjunctions identified as red-level risks (i.e., those with $\bar{P}_c \geq 10^{-4}$).

To demonstrate how collision and fragmentation probabilities can be used together, a threshold of $F = 10^3$ was used to assess an unacceptably high level of risk to the orbital environment. Figure O-5 compares fragmentation and collision probabilities for known-on-unknown CARA conjunctions, calculated using this fragment production threshold. Among the conjunctions analyzed, 1,734 represent red-level close approach risks with $\bar{P}_c \geq 10^{-4}$. Among these, 122 (or 7%) also have $\bar{P}_F \geq 10^{-4}$, so they represent red-level environmental risks as well. Figure O-5 plots these dual high-risk conjunctions as red stars, illustrating how collision and fragmentation probabilities can be used together to identify the subset of events with the highest spacecraft and environmental risks. Pink diamonds and triangles represent conjunctions with red-level close approach risks, but lower environmental risks.

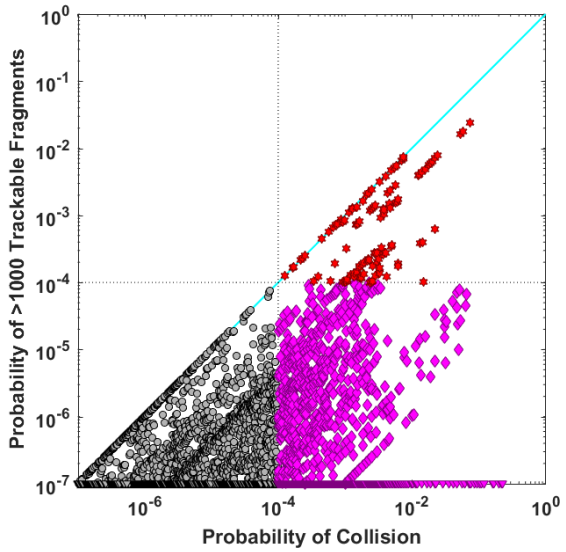

Figure O-5 Collision and Fragmentation Probabilities for Known-on-Unknown Conjunctions[28]

As discussed above, a fragment production threshold of $F = 10^3$ indicates that 7% of the analyzed known-on-unknown conjunctions with $\bar{P}_c \geq 10^{-4}$ also have $\bar{P}_F \geq 10^{-4}$. This analysis uses $F = 10^3$ as a threshold number of trackable fragments because such a collision would potentially represent a major source of LEO debris generation, comparable to the Iridium-Cosmos collision in 2009 which produced about 1,200 trackable fragments that remained in Earth orbit for longer than one year. Other production thresholds provide different assessments of environmental risk in a non-linear fashion. For instance, about 20% of the studied conjunctions have $\bar{P}_F \geq 10^{-4}$ for the somewhat more moderate threshold of $F = 10^2$. So, considering the range of $10^2 \leq F \leq 10^3$ indicates that 5% to 20% of the high mission risk conjunctions also could be assessed to pose an elevated risk to the orbital environment.

It must be emphasized that no O/O would be asked to take advantage of the low-debris-producing-event possibility for relaxed mitigation requirements. Whether to focus on the protection of their own payload or merely to take a more conservative posture generally, missions certainly may embrace the 10^{-4} Pc threshold for all conjunctions. From an orbit regime protection point of view, however, it would not be unreasonable to relax this threshold mildly for situations that are non-catastrophic and only expected to create a small amount of debris, especially in the presence of other relevant considerations, such as the inability to identify a truly adequate mitigation action that did not impose non-trivial mission compromise. The use of fragmentation propensity may also be desirable for triage situations in which a mission is experiencing more serious conjunctions than it is possible to remediate. In such cases, one could direct mitigation focus to those conjunctions that hold the greatest debris production potential.

[28] From Hall and Baars (2022)

Appendix P. Event Actionability

P.1 Introduction

Although widely used, the term "conjunction event actionability" is a somewhat unfortunate term because it implies a broader scope than it merits. Its precise meaning is the assessment of the propagated state and state uncertainty information for the two satellites in conjunction (but with the focus usually on the secondary object) to determine whether these data constitute a reasonable basis for conjunction risk assessment and mitigation actions. It does not include the further step of deciding, in the presence of a high-risk situation, whether the mitigation actions are excessively invasive or detrimental to the mission's objectives to warrant their being set aside despite the collision risk; that is, whether an O/O would be justified in refraining from taking "action" to mitigate the conjunction and lessen the collision risk because of the mission impact of the mitigation action. This latter consideration is real and constitutes part of the risk assessment process, but one arrives at this decision point only after determining that the orbital data feeding the analysis are durable and thus are enabling credible collision risk calculations.

The propriety of considering the quality of the event's input orbital data is obvious because an O/O will certainly wish to certify that the collision risk is truly high and that a proposed mitigation action will remediate the collision risk before considering its actual execution. The desire for a conservative risk approach does not make the problem simpler. If the input astrodynamics data are questionable, it is also questionable whether any proposed mitigation action will actually improve the situation because such an action could in fact make the situation worse. So it is not appropriate simply to say that situations of questionable data quality should, out of conservatism, be afforded such actions if the calculated risk parameters exceed the threshold for mitigation actions. Rather, it is necessary to establish a method for identifying those cases in which the input data may be sufficiently poor to make meaningful risk assessment impossible.

It is important to recognize that the question to be addressed here is whether the orbital data properly represent the two objects' states and uncertainties and not whether the associated uncertainties are large or "too large." If one embraces Pc as the principal (but not necessarily the sole) collision likelihood assessment metric, excessively large covariances have the effect of depressing the Pc value and thus giving a (much) lower statement of risk. This particular phenomenon, called the "dilution region" situation, is a known peculiarity of Pc and is discussed at some length in Appendix M, but there is general agreement that high Pc values do represent situations of high collision likelihood. In such situations, the fact that covariances may seem excessively large should not constitute an impediment to event actionability. If, despite a somewhat tracking-data-impoverished situation (hence the large covariance), a worrisome Pc is still produced, *a fortiori* the situation should be treated as serious and worthy of mitigation.

This area of conjunction risk assessment—the determination of event actionability—possesses the least precision in terms of clear, documentable standards. The certification of orbit-determination updates as valid and reasonable and propagation intervals and methods as sufficiently representative is, in the end, rendered not through conformity to strict, fully

articulated rules but rather through the judgment of expert orbital analysts who have personally performed thousands of orbit-determination updates and propagations. Astrodynamics is often at least as much an art as a science, and batch orbit-determination update particularly so. To be sure, most of the cases that are actually encountered in conjunction assessment practice can be judged to be valid and acceptable through rule conformity alone, and there are certain cases that are so poor that there is little difficulty in recognizing their invalidity immediately. But there is also a relatively small input data group that cannot be directly assigned to either of these resolutions, and it is here that expert opinion is required.

There are two separate aspects of the astrodynamics input data to consider: the states and covariances for the primary and secondary objects at epoch as outputs of the orbit-determination process, and the states and covariances propagated forward to TCA. These two aspects will be treated separately below, with the concluding section outlining how considerations from each are combined into a judgment of actionability/non-actionability for a particular event. Some of the threshold values for the actual parameters used in the tests to be described below are placed in an annex to this appendix, both for ease of reading and to allow easier document update should these values be modified. Finally, while it is the case that in principle a judgment of the suitability of the primary object's state and covariance is required as part of the overall actionability assessment, in practice it is almost always the secondary object's data quality that is an issue. To simplify the treatment, the following discussion will frequently frame the discussion in terms of a single object that can be presumed to be the secondary.

P.2 Evaluation of the Propriety of the Orbit-Determination Fit

It should be obvious that a quality orbit-determination fit for the object is a foundational element in any use of its state and uncertainty data. If the fit itself is questionable, it is difficult to have confidence in any astrodynamics products propagated forward from it. Because the USSPACECOM catalog is at present usually the sole supplier for all data on the secondary object (especially in the case of debris objects with a small radar cross section value) and also provides solutions for the primary object, the focus has to be placed on the orbit-determination fit mechanism used for this catalog, which is not a sequential estimator but a minimum-variance batch process. This means that in addition to the force model settings for the dynamical models, the time-span of the tracking data for the fit, data density, tracking data sensor composition, and retention of the sensor data used in each batch update have to be considered. If a different data provider for orbital information about the secondary object were to be used, a set of orbit-determination quality criteria tailored to that particular provider's orbit-determination methodology and engine would need to be developed and consulted. The remainder of this section can be seen as a proposed template for how that development and consultation might proceed.

If it were possible to generate hard-and-fast rules for determining the control settings and data handling for these batch updates, the assessment of fit acceptability would be much more straightforward. Despite decades of attempts, astrodynamics specialists for DOD have concluded that such a rule set is simply not possible, especially when densely-packed debris clouds are considered. The only way truly to evaluate the propriety of an orbit-determination fit is a manual

review by an expert. This individual has access to information of the full suite of input sensor raw and "management" data including:

- Tables of residuals,
- Residual plots in a variety of different constructions and the ability to edit out individual observables,
- Before-and-after values of key orbital elements in the context of long-term plots to evaluate trends, and
- The ability to attempt multiple corrections with different force-model settings and data contents to evaluate the results comparatively and choose the best outcome.

Such evaluations, most of them visual, simply cannot be replaced by rules themselves.

However, what is possible is to provide a set of guidelines that, if violated, would typically prompt a manual review by an expert. Within a NASA or USSPACECOM context, an expert could be summoned and, with access to the data products enumerated in the above paragraph, could render an expert opinion on the propriety of the orbit determination. Outside of these agencies, such data access is not available. Nonetheless, the rule set can be useful; for example, orbit-determination results that do conform to all of the general rules can, with a high degree of confidence, be accepted as a basis for conjunction risk assessment.

The following subparagraphs describe the particular orbit-determination input summaries, settings, and quality factors evaluated by the rule set, and the annex to this appendix gives threshold values that allow for the evaluation of an orbit determination's conformity to these rules. All the information needed to evaluate a particular orbit determination is present in the CDM.

P.3 Force Model Settings and Non-Conservative Force Model Parameter Values

Any space catalog has at its core a set of astrodynamics dynamical models that are used to predict the trajectories of space objects, and the orbit-determination process determines parameter values to use within these models to predict future positions of a particular satellite. Different physical phenomena and their effects on satellites are modeled, and for some of these models, varying levels of fidelity can be selected. The following paragraphs list each of the selectable force models that can be applied, identify the selection criteria, and give some indication of parameters and parameter values that might lead one to question the propriety of an orbit determination.

1. **Geopotential**. Two-body motion, the simplest of possible orbit solutions, is the foundation of the astrodynamics model set. The first major improvement in precision is the recognition that the Earth is not a uniform and uniformly dense sphere but varies from this idealization in many ways. A spherical harmonic representation of the actual geopotential is used to represent the Earth's bulge at the equator and other density non-uniformities; the spherical harmonic order is specified as part of the correction. The minimum required geopotential order (in terms of zonals and tesserals) for an acceptable

fit is determined by considering characteristics of the satellite's orbit, and any orbit-determination update that uses a geopotential order lower (smaller) than this specified value is flagged for manual review. The actual minimum geopotential order thresholds as a function of orbital parameters are given in the annex to this appendix.

2. **Lunar-Solar Perturbations.** While the Earth is obviously the most significant central attracting body for a satellite, the sun and moon are large enough to visit a non-negligible effect on a satellite's orbit. For precision solutions, this modeling (called "third-body effects") should always be engaged.
3. **Solid Earth Tides**. The gravitational force of the moon deforms the quasi-spherical Earth, and this deformity changes the geopotential and satellite orbits. Often, the effect is small and unlikely to alter conjunction assessment results. Because it is not computationally difficult to characterize, it is standard practice to include this modeling input in precision solutions. In the main, however, it is unlikely that the failure to include this perturbation would make the resultant orbit determination questionable from a conjunction assessment perspective although it could alter the results observably.
4. **Atmospheric Drag**. The major non-conservative force affecting many LEO orbits is atmospheric drag. The modeling of drag acceleration is a function of the satellite's velocity relative to the atmosphere, the atmospheric density, and the satellite's ballistic coefficient, which itself is a combination of the coefficient of drag, the satellite's frontal area, and its mass. Because for most satellites, especially debris objects, neither the drag coefficient nor the frontal area nor the mass is known, the entire ballistic coefficient is treated as a single solved-for parameter as part of the orbit determination. Certain LEO orbits should include atmospheric drag modeling and solutions for the ballistic coefficient, and for those that do, there are ranges of reasonable solutions for this solved-for parameter. The annex to this appendix delineates the LEO orbits that require a drag solution and the ranges of acceptable ballistic coefficient values.
5. **Solar Radiation Pressure**. While electromagnetic radiation has no mass, it does impart momentum, and the momentum carried by the sun's energy and incident upon the satellite has a discernable effect on the resultant orbit. The USSPACECOM dynamical model set employs a standard solar radiation pressure model (SRP), which is a function of a solar radiation pressure coefficient (SRPC) (analogous to the ballistic coefficient) and a scalar and vector distance to the sun. Certain orbits should have the solar radiation pressure model enabled, and for these there are acceptable ranges of values for the solar radiation pressure coefficient. The relevant orbits for solar radiation pressure compensation and the associated ranges of values for the coefficient are given in the annex to this appendix.

P.4 Orbit Determination Fit Span (or Length of Update Interval)

Sequential estimators process each measurement individually, usually as each is received; batch estimators collect a "batch" of measurements and process them as a group. When using batch estimation, it is necessary to identify the particular group of measurement data to be fit, which usually means determining the period back in time from the present for retrieval of data to use in

an update. While this activity may at first not seem important, in fact it can greatly affect the quality of the resultant orbit determination. If the data period is too long, the prediction error from the orbit-determination fit state is increased; if the data period is too short, a robust drag or solar radiation pressure solution is not possible; and if there are too few measurements contained within the span, the solution is not reliably representative.

To set the data interval and density correctly, the USSPACECOM batch update process employs a complicated algorithm called the Dynamic Length of Update Interval (LUPI) Assignment (DLA) to examine the measurement data history for each fit and assign the proper LUPI to strike an acceptable balance between maximizing prediction accuracy and ensuring a reasonable solution for the non-conservative force parameters (drag and solar radiation pressure). The algorithm operates by beginning with the maximum acceptable LUPI for a particular orbit and attempting to minimize it while preserving sufficient observational data to endure a quality update, and if the maximum LUPI itself does not encompass enough tracking data, the algorithm will expand past this theoretical maximum value to attempt to bring more data into the correction. The goal of this approach is to provide quality updates most of the time and serviceable updates all the time, with "serviceable" defined here as sufficient to allow sensor reacquisition of the satellite. Updates that are merely serviceable are, however, not in themselves of sufficient quality for conjunction risk assessment. Also worrisome are LUPI lengths shorter than the default minimum, which occur when large amounts of measurement data are eliminated from a satellite's history (due, for example, to a satellite maneuver after which the old observational data have to be thrown away because they no longer represent the satellite's current trajectory). While a subject matter expert could, with broader data access, perhaps certify some of these results as acceptable for conjunction risk assessment, as a general rule, orbit determinations with LUPI lengths that are either longer than the theoretical maximum or shorter than the theoretical minimum cannot produce reliable state updates and reliable covariances and thus cannot serve as a basis for conjunction risk assessment.

A table of these maximum and minimum lengths is given in the annex to this appendix.

P.5 Residual Acceptance

The batch solution generates an optimal solution by minimizing the sum-of-squares residual of the data chosen for the fit; therefore, large residuals against individual observables affect the fitting process substantially. Because it is not uncommon to receive "bad" measurement data from sensors, a stratagem has been implemented to limit the overall effect of potentially errant data: between iterations of the non-linear regressive solver, the measurement residuals against the provisional solution are examined, and data points that manifest excessively large residuals are eliminated. This allows the fit to proceed without being influenced disproportionately by only a few measurements.

The elimination of measurement data in a data-fitting context merely because they appear to encumber a more satisfactory fit is always somewhat disconcerting as most numerical analysts discourage the elimination of any given datum without some *a priori* reason to suspect that it may be errant. However, incidences of satellite cross-tagging (in which the assignment of data to the correct satellite miscarries by the data being assigned to some other, usually nearby satellite)

are frequent enough that some provision has to be made for eliminating sensor observations that simply do not seem consistent with the rest of a satellite's measurement data. There are also situations in which data mismatches are overtly recognized, such as after a satellite maneuver, because the trajectory has changed impulsively and observational data before the maneuver do not represent the current trajectory and have to be eliminated intentionally.

If too much of the measurement information is eliminated, the concern is that the fit may not be properly representative. Therefore, when the percent of the residuals eliminated exceeds a certain value, the fit merits manual review. A table of these values is given in the annex to this appendix.

P.6 Weighted Root-Mean-Square of Residuals

It is common when performing an iterative batch fit to use the root-mean-square of the residuals as an indication of fit quality, tracking this value to ensure that the fit is improving with each iteration. For an unweighted root-mean-square, the ideal value would be zero as it would indicate that the model fits the data exactly without any residual error. For the USSPACECOM minimum-variance batch solver, a weighted root-mean-square is used (WRMS), in which the square of each residual is divided by the variance of the *a priori* expected error for that observable type (e.g., range to target, azimuth angle, elevation angle) from that particular sensor as established by a sensor calibration process separate from the orbit-determination activity. If the residual errors and actual sensor errors are Gaussian, then the average of these ratios should equal unity (as will its square root). The weighted root-mean-square is a better measurement of fit error because the best reasonable expected outcome is that the error of the fit will be of essentially the same magnitude as the inherent error in the observations.

If the fit's weighted root-mean-square is too large, then the fit is not particularly convincing, and manual review would generally be counselled. A weighted root-mean-square value less than unity, while not necessarily bad, nonetheless would also warrant a manual review: while a fit of a higher quality than the inherent error in the observations is possible, it is usually a result of too few data in the orbit determination and therefore should be investigated. Thresholds for excessively high weighted root-mean-square are set by object type and given in the annex to this appendix.

P.7 Default Covariance

The DOD precision orbit-determination solution produces an estimation error covariance as a regular product. There are situations, however, in which the automatic precision orbit-determination solution cannot be made to converge, and in such cases, the system executes a general perturbations analytic orbit-determination solution, employing the same theory used to produce TLEs. This process as presently designed produces a state (although an inaccurate one with 1-2 km of expected error in LEO) but no covariance, and this is indicated by providing a diagonal covariance for which the diagonal elements for the position portion are each ten Earth radii.

General perturbation solutions are not sufficiently accurate to serve as a basis for conjunction mitigation actions, so if one of these default covariances is encountered, the state data that accompany it are not suitable for conjunction risk assessment.

P.8 Review Process

As stated above, if the full orbit-determination data are present and a subject matter expert is available to render an expert opinion, situations in which the general rules given above are violated can be investigated and an adjudication obtained. If this level of access is not available, the above rules can serve as a one-sided test; namely, if the current orbit determination conforms to all of the rules, then it can be presumed that the orbit determination is durable and can serve as a basis for conjunction risk assessment and, if necessary, mitigation action planning.

P.9 Evaluation of Propagation from Epoch to TCA

Most conjunction risk assessment approaches make assessments using the states and covariances of the primary and secondary objects propagated to TCA, so in addition to considering the propriety of the orbit-determination fits themselves, one also has to consider whether any issues with the propagation itself might make the TCA products unsuitable for conducting risk assessment. Issues related to propagation are often called out as potentially problematic, and a treatment of each of these is given in this section. But the overall conclusion is that the USSPACECOM approach to producing astrodynamics products at TCA is robust and contains mechanisms to address the major sources of expected propagation error, and these can be augmented with additional processes within risk assessment. As such, if an orbit determination sustains the criteria for an acceptable fit, it can be presumed that this fit propagated to TCA renders a state and covariance acceptable for conjunction risk assessment, except in a few narrow instances called out below.

P.9.1 Propagated Covariance is Defective

In some situations, the propagated covariance can be defective to the degree that it cannot be used as presented for conjunction risk assessment.

1. **Null Covariances**. The first is a null covariance in which all the entries are zeroes. This is the equivalent of not having a covariance at all, and when described in the previous section that addressed orbit-determination fit results, it was pointed out that situations with such a covariance cannot be used for conjunction risk assessment. If there is no covariance at epoch, there cannot be a propagated covariance at TCA either, so such a situation can be considered to be inactionable. It is possible to use maximalist techniques such as those developed by Alfano (2005b) and by Frisbee (2015) to proceed in situations in which only one of the two objects has a covariance, but these techniques are exceedingly conservative and therefore not recommended as a routinely used proxy for collision likelihood.
2. **Default Covariances**. The second is a default covariance in which the presence of diagonal elements of ten Earth radii indicates a general perturbation solution that produced no covariance. While in principle this covariance can be propagated to TCA, it will essentially be an “infinite” covariance at TCA—just as it was at epoch—and therefore force any calculated Pc to zero (and sometimes introduce convergence problems in Pc calculation routines). Situations such as this can be judged to be non-actionable (because the covariance for one of the objects cannot be established) or

produce in every case a Pc of zero (because this is what very large covariances do). Embracing either possibility leads to the same conclusion of not requiring a mitigation action.

3. **Non-Positive-Semidefinite Covariances**. The third is for the TCA covariance to become non-positive-semidefinite. This issue is addressed at greater length elsewhere (Hall et al. 2017b), and the takeaway from that discussion is that the problem arises due to truncation and interpolation errors (not fundamental problems with the orbit determination) and can be straightforwardly repaired. The article recommends certain repair techniques, and the source code for them is provided on the NASA CARA software repository. (See Section 7, Contact Information in this document for the specific URL.) A modification to the USSPACECOM operational system has been implemented that should essentially eliminate non-positive-semidefinite situations.

Of the mainstream direct defects in TCA covariances, null and default covariances do produce situations that result in inactionability; non-positive-semidefinite covariances do not.

P.9.2 Excessive Propagation Interval to Retain Gaussian Covariance Behavior

The astrodynamics discipline has had to address the question of Gaussian uncertainty volumes and the difficulties introduced by the Cartesian framework's inability fully to represent curvilinearly produced results. As discussed at greater length in Appendix N, while this debate continues in the critical literature, the conjunction assessment enterprise has been able largely to set it aside by recognizing that the issue is not really relevant to high-Pc events because of the amount of overlap of the "main" portions of the covariance necessary to produce a high Pc. Furthermore, the issue can be remediated easily by performing Monte Carlo from TCA with the random sampling conducted from the equinoctial representation of the covariance. While much has been made in the literature of the problem of non-Gaussian covariances for conjunction assessment, based on NASA CARA's analysis, this problem is not crippling for the categories of events that actually matter to conjunction risk assessment, and in any case, it can be addressed with a particular Pc calculation technique that is both straightforward and tractable.

P.9.3 Excessive Propagation Interval Due to a Lack of Tracking Data

The USSPACECOM orbit-determination process places the epoch time of its orbit-determination fits at the time of the last observation. Since this is the time at which the fitted results are modeled, any propagation into the future takes place from that time. Because this orbit determination is used as the most current update until more tracking data are received and a new update executed, to propagate the state and covariance to TCA usually involves two stages: to propagate forward from the epoch time to the current time, and then to propagate from the current time forward to TCA. If no new tracking data are received for some time, then a quite long propagation of the original orbit-determination state may be required. For example, if the object has not been tracked for five days and TCA is three days from the present time, a total of eight days' propagation is required to produce the state and covariance at TCA.

It is best if tracking data are received frequently because this produces better data density for the fit and reduces the overall amount of propagation time. There is nothing about long propagation times *per se* that indicts the utility of the resultant products; as the propagation proceeds, the uncertainties in the propagated covariance grow appropriately to represent the expected uncertainties of the states at the propagation termination, which is here TCA. Additionally, adjustments to the covariance to account for atmospheric density forecast error and satellite frontal area uncertainty are included and contribute to the propagated covariance's growth (discussed in Appendix N). Finally, a large covariance matrix will in most cases depress the calculated Pc value, naturally correcting for a situation in which the state uncertainties are so large that it may not be comfortable to use them as a basis of action. Given this dynamic, the lack of recent tracking data invalidates neither the original fit (presuming there was sufficient tracking in the fit-span to produce an acceptable fit) nor the propagation to TCA.

Nonetheless, a rule of thumb that has been used over the last few decades for orbit-determination batch updates is that the propagation interval should not be longer than the fit-span/LUPI. It is generally considered dangerous to try to propagate longer than the span of measurement data that directed the orbit-determination update. While there are undoubtedly situations in which propagations of this type could still be representative, it is believed that the reasonable span of the orbit determination has been exceeded in such a case, and it is thus reasonable to refrain from any mitigation action for conjunctions for which either object's orbit determination at TCA was generated with so extended a propagation interval.

P.9.4 Excessive Atmospheric Density Error Due to Solar Storms

As explained in Appendix N, for some years, the USSPACECOM orbit-determination process has adjusted the covariance in the CDM for anticipated atmospheric density forecast error through the application of a consider parameter. The Jacchia-Bowman-HASDM 2009 (JBH09) atmospheric density model used by USSPACECOM contains special functionality to reduce propagation error in the presence of Coronal Mass Ejections (CMEs), a commonly encountered type of solar storm. A special model given the name "Anemomilos" attempts to predict the size, time of arrival, and geoeffectiveness of CMEs, and the atmospheric density is modified appropriately during the prediction interval to reflect the storm's predicted arrival and effects. (Tobiska et al. 2013) Paired with the appropriate consider parameter value, which will compensate for the expected uncertainty in this type of modeling, the predicted product should in principle account for atmospheric density mismodeling. The fact that the solar environment is perturbed should not, therefore, result in an *a priori* conclusion that the predictions of an event's severity are errant and that a claim of event inactionability is appropriate. Having said that, it is also the case that the performance of the Anemomilos model during the most recent solar cycle (solar cycle 25) has been disappointing: normed on data from earlier solar cycles, the model is not producing representative results presently. A number of different mitigation activities are presently being considered, including simply turning off this particular modeling feature. Unfortunately, it is not possible during regular operations to determine the degree to which Anemomilos is affecting prediction outcomes, although this model will engage only when the predicted Disturbance Storm Time (Dst) parameter value is smaller than -75nanoTeslas, so one can consult space weather predictions to determine whether there is any possibility of the

model's being employed. This general issue is addressed at greater length in the walk-through of a sample event in Appendix Q.

Some additional insight into such situations can be gained by constructing what are called Space Weather Trade Space (SWTS) plots that explore how the collision likelihood of a particular event would change if the atmospheric density were mismodeled. Because atmospheric density and ballistic coefficient are multiplicatively coupled in the atmospheric drag acceleration equation, changing one of these parameters has the same effect as changing the other. It is thus possible to vary the primary and secondary objects' drag parameters to understand the effect of drag modeling on the event's conjunction likelihood.

The plots are constructed by varying the nominal ballistic coefficient by half an order of magnitude in each direction with the x-axis giving the primary object ballistic coefficient variation, the y-axis that for the secondary object, and the color indicating the resultant Pc value. However, these details are not so important because it is the overall morphology of the figure that is meaningful. In Figure P-1**,** despite large variations in the ballistic coefficient (as a proxy for atmospheric density), the Pc changes little. This event is not sensitive to space weather mismodeling, and thus actionability is not strongly affected by solar storm developments and potential mismodeling.

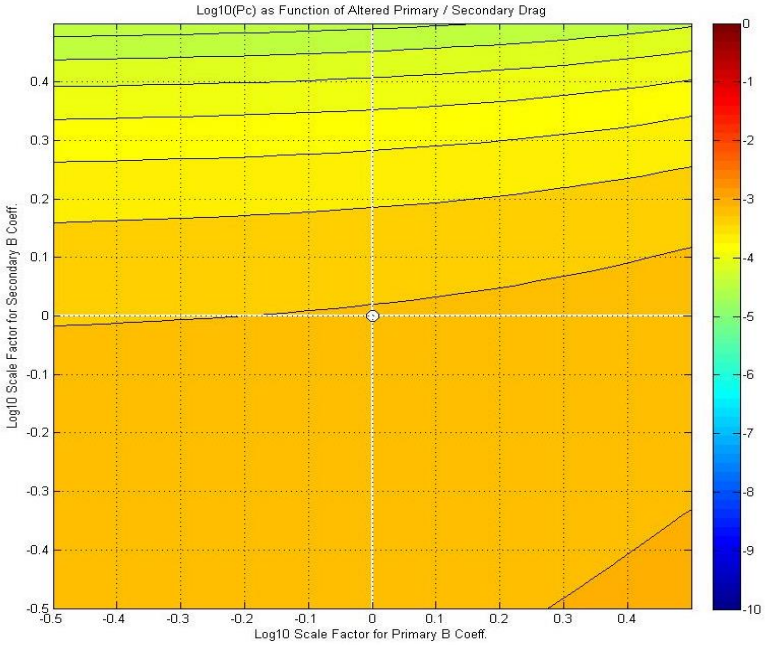

Figure P-1 SWTS Plot for Invariant Situation[29]

In Figure P-2, the current Pc, as represented by the center point of the figure, lies on a "ridge" of high Pc values; any atmospheric drag mismodeling that moves the situation off the center point

[29] From Hejduk et al. 2017.

will result in a lower rather than higher Pc. So, if the current Pc is below the threshold that would require a mitigation action, the event should still be safe even in the presence of model error.

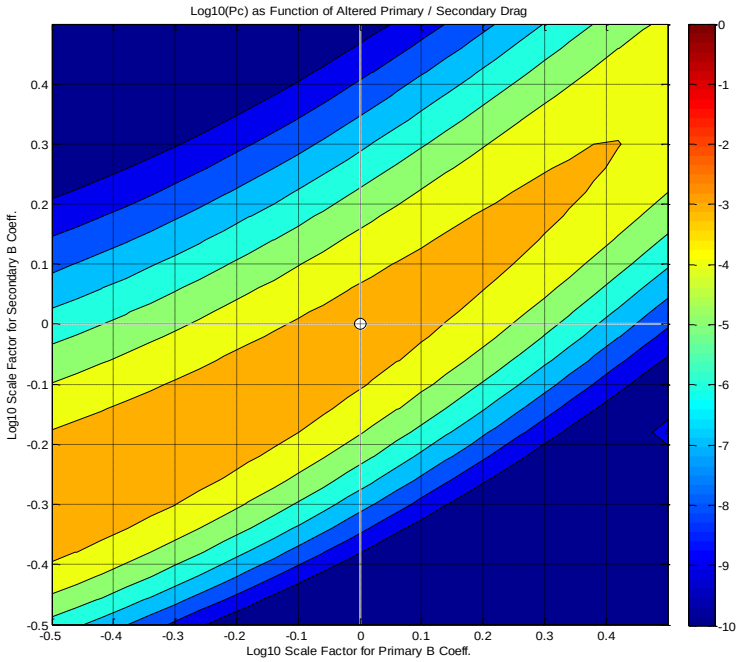

Figure P-2 SWTS Plot for "Ridge" Situation[30]

Finally, in situations in which the Pc is not on a ridge and where non-trivial variation is observed, then model error could either increase or decrease the Pc, as shown in Figure P-3. In such cases, one is left without the reassurance of either of the two previous examples. However, given that the estimation process attempts to take account of drag uncertainty through modeling even of solar storms, the CDM result is presumed to represent the best estimate possible and, in the absence of other indicting data, is expected to be reliable and actionable.

[30] From Hejduk et al. 2017.

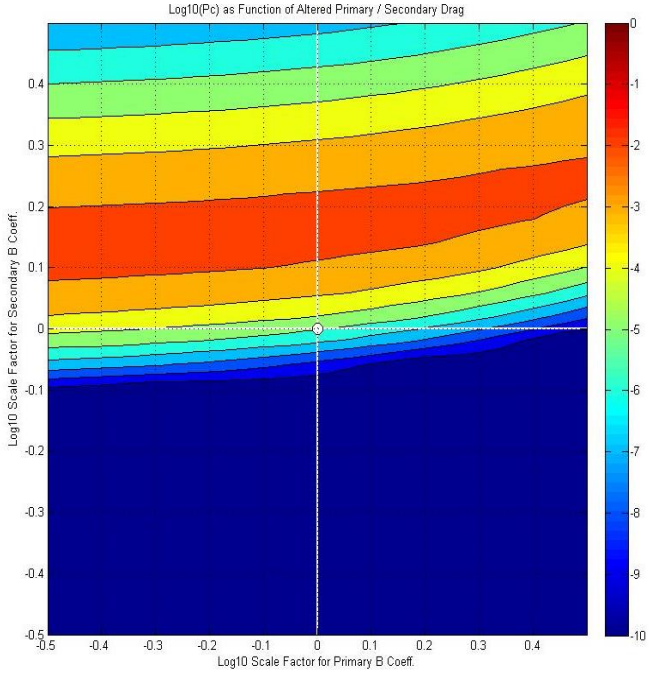

Figure P-3 SWTS Plot for Variation Situation[31]

P.10 Summary

As the previous discussion indicates, the orbit determination and propagation process nearly always produces data that can be considered actionable. There are certain indications that an orbit-determination fit may potentially fall short, and an even smaller number that would counsel the dismissal of an orbit determination as the basis for conjunction risk assessment. It is similarly infrequent that the propagation results to TCA can be questioned, and these situations can usually be addressed in other ways (e.g., the repair of a non-positive-definite covariance). In both situations, there are additional one-sided tests that, if passed, can reassure the user about the propriety of the data and its ability to subtend conjunction risk assessment.

[31] From Hejduk et al. 2017.

P.11 Annex

This annex provides specific thresholds for the orbit-determination quality checks.

Table P-1 Geopotential, Atmospheric Drag, and Solar Radiation Pressure

Perigee Height (km)	Eccentricity	Object Type	Geopotential Zonal and Tesseral	Solve for Drag?	Solve for Solar Rad. Pressure?
0 < p < 500	< 0.25	Payload	36	Y	N
		Rocket Body / Platform	36	Y	N
		Debris/Unknown	36	Y	N
500 < p < 900	< 0.25	Payload	36	Y	Y
		Rocket Body / Platform	36	Y	Y
		Debris/Unknown	36	Y	Y
900 < p < 2000	< 0.25	Payload	24	Y	Y
		Rocket Body / Platform	24	Y	Y
		Debris/Unknown	24	Y	Y
0 < p < 500	> 0.25	Payload	36	Y	N
		Rocket Body / Platform	36	Y	N
		Debris/Unknown	36	Y	N
500 < p < 1000	> 0.25	Payload	24	Y	Y
		Rocket Body / Platform	24	Y	Y
		Debris/Unknown	24	Y	Y
1000 < p < 2000	> 0.25	Payload	18	N	Y
		Rocket Body / Platform	18	N	Y
		Debris/Unknown	18	N	Y
2000 < p < 10000	any	Payload	12	N	Y
		Rocket Body / Platform	12	N	Y
		Debris/Unknown	12	N	Y
p > 2000	any	Payload	8	N	Y
		Rocket Body / Platform	8	N	Y
		Debris/Unknown	8	N	Y

Table P-2 Ballistic Coefficient and Solar Radiation Pressure Coefficient Reasonability

Energy Dissipation Rate (w/kg)	Object Type	Ballistic Coefficient		Solar Radiation Pressure Coefficient	
		Min	Max	Min	Max
< 0.0006	Payload	0.001	0.1	0.001	0.1
	Rocket Body / Platform	0.001	0.2	0.001	0.2
	Debris/Unknown	0.001	1	0.001	1
> 0.0006	Payload	0.001	0.1	0.001	0.1
	Rocket Body / Platform	0.001	0.2	0.001	0.2
	Debris/Unknown	0.001	1	0.001	1

Table P-3 LUPI Minimum and Maximum Values

EDR Min	EDR Max	e	Length of Update Interval (days)	
			Lower Bound	Upper Bound
0	0	any	14	See graph
0+	0.0006	< 0.25	3.5	18
		> 0.25	14	See graph
0.0006	0.001	any	1.5	17
0.001	0.0015	any	1.5	15
0.0015	0.002	any	1.5	14
0.002	0.003	any	1.5	12
0.003	0.006	any	1.25	11
0.006	0.009	any	1.25	10
0.009	0.015	any	1.25	8
0.015	0.05	any	1.25	8
0.05	0.05+	any	1.25	7

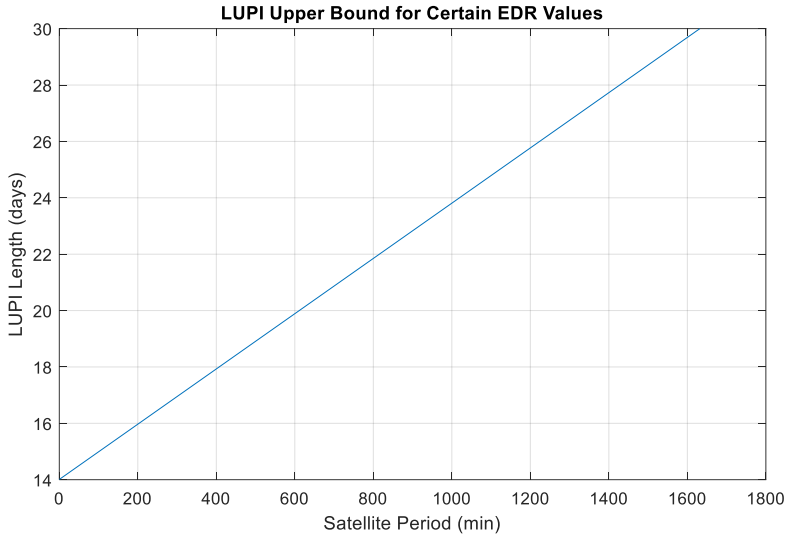

Figure P-4 LUPI Upper Bound for Certain EDR Values

- **Residual Acceptance**. Fewer than 80% residual acceptance would generally prompt manual review of an orbit determination.
- **Weighted Orbital-Determination Residual Root-Mean-Square**. Weighted root-mean-square values exceeding the following thresholds are considered excessive:

  Payload: 1.5

  Rocket Body / Platform: 2.0

  Debris/Unknown: 5.0

  No thresholds for sub-unity weighted root-mean-square levels have yet been established.

Appendix Q. Notional Display Flow for Conjunction Event Processing

Q.1 Introduction

While appendices E through P in this Handbook address many of the technical aspects of the conjunction event processing discipline, this appendix illustrates how the individual pieces come together to perform on-orbit conjunction risk assessment. The operational orbital safety process is illustrated through a series of graphical displays that conjunction risk assessors use to determine whether a mitigation action is warranted for a particular conjunction and, if it is, what sorts of such actions might be effective in adequately reducing the collision risk.

The graphical displays in this appendix are a subset of those used by the NASA CARA group to perform risk assessment in protection of NASA's fleet of non-human space flight satellites, and the examples presented are for a recent actual event that resulted in the planning and execution of a mitigation action. To facilitate public release of the information, neither spacecraft is specifically identified, and the orbital data have been slightly altered.

NASA executes conjunction assessment screenings of its assets against the DOD space catalog once every eight hours, and for the orbit regime that contains the particular protected asset in use in this example, a screening volume of 0.5 km x 17 km x 20 km was used. This particular conjunction appeared at the 6.5 days-to-TCA point, which means that it was essentially identified as early as possible (using 7-day predicted ephemerides for the primary object). Because the initial Pc was greater than 1E-07, this event was in "yellow" status from the very beginning, meaning that the collision likelihood was high enough to merit close attention as the event developed. As such, the conjunction risk assessment process was engaged from the beginning.

The displays in this appendix follow this event from initial detection to the mitigation action commitment point, which for this event was one day prior to the time of the closest approach. Commentary is provided for each display, and since there is always more that can be said about each display, the commentary is reasonably abbreviated and focused on the most salient points of each presentation.

Q.2 Primary and Secondary Object Background Information

In making a risk assessment determination, it is important to have information about the orbits and maintenance history of the primary and secondary objects as background. Different orbits have different properties and expected stability, and maintenance histories and parameters testify to the quality of the orbit determination available to analyze this event. It is helpful to display these data in consolidated form so that the parameters of interest can be viewed and apprehended quickly.

Q.2.1 Primary Object Information

Table Q-1 provides the orbital and orbit determination estimation information for this conjunction's primary object.

Table Q-1 Primary Satellite Vital Statistics

Orbital Information at TCA

Orbital Parameter	Value
Period (min)	97.6
Perigee Height km)	681.3
Apogee Height (km)	721.7
Inclination degrees)	98.2
EDR (W/kg)	2.77e-04
RCS	Large (>1m^2)

Estimation Specifics

Parameter	Value
Avg. Tracks Per Day	5.7
Num. Obs. In Span	237
Time of Last Observation	<24 hours
WRMS	1.55
Ballistic Coefficient (m^2/kg)	0.027
SRP Coefficient (m^2/kg)	0.005

In most cases, the primary object is much better maintained than the secondary object, meaning that the primary object's orbit determination information is generally good and therefore not determinative in assessing the event's overall data quality. Furthermore, if the object is screened using the owner/operator (O/O) ephemeris, there will typically not be any available orbit determination estimation information at all. But it is helpful to examine whatever information is available for the primary object to make sure the situation is well understood.

One observes that the primary is in a nearly circular, sun-synchronous LEO orbit with an average altitude of about 700km. The energy dissipation rate (EDR) value indicates that, while drag has an effect, it is relatively mild. The altitude is such that both drag and solar radiation pressure (SRP) should be modeled, and the two resultant solved-for values are reasonable. (Consult Appendix P for acceptable ranges of values for parameters such as this.) The weighted root mean square (WRMS) value here is low enough not to raise any objection. The tracking density is reasonably large, and tracking data has been included in the orbital solution that was collected within the last day, so propagation to TCA will not have to extend very far into the future.

Overall, this primary satellite is well maintained and not propagated excessively, so there is nothing to indicate any problems with the fit or propagation.

Q.2.2 Secondary Object Information

Basic orbital and orbit determination estimation information for the secondary object is shown in Table Q-2.

Table Q-2 Secondary Satellite Vital Statistics

OBJECT - Orbital Information @ TCA

Orbital Parameter	Value
Period (min)	98.7
Perigee Height (km)	674.9
Apogee Height (km)	718.5
Inclination (degrees)	81.2
EDR (W/kg)	5.19e-03
RCS	Small (< 0.1m^2)

OBJECT - Estimation Specifics

Parameter	Value
Avg. Tracks Per Day	0.5
Num. Obs. in Span	15
Time of Last Observation	< 48 hours
WRMS	3.41
Ballistic Coefficient (m^2/kg)	0.682
SRP Coefficient (m^2/kg)	0.285

OBJECT - Event Flags

Event Flag	Status
Single Station Tracking	Y
Increased Tasking Requested	Y
Increased Tasking Received	Y
State Update Consistency Check	Y

The orbit of the secondary object is not substantially different from that of the primary, although the inclination is somewhat lower. However, due presumably to a different area-to-mass ratio, the drag influence is much higher for the secondary object: the high EDR value indicates a significant drag effect, and this is confirmed by the large solved-for ballistic coefficient. The orbit altitude indicates that SRP should be solved for as well, and it is: the large value here also indicates a high area-to-mass ratio. The tracking levels for the secondary object are poor: 0.5 tracks/day is an order of magnitude smaller than the tracking density for the primary.

Examining the Conjunction Data Message (CDM) (not shown here) reveals that the 15 observations (obs) used in the latest orbit determination update for this object span a 9.5-day period. Thus, while the overall tracking situation is not the best, the length of the update interval (LUPI) is only half the maximum value and therefore tolerable. (Consult Appendix P for information about the LUPI parameter.) The fact that all the tracking comes from a single sensor is undesirable, but it is a circumstance that is observed occasionally with small debris objects, which this is given its radar cross section (RCS) value. The WRMS is high but below the quality threshold of 5 for a debris object. Data in the CDM also indicates that the propagation time to TCA is not all that long (a few days) and certainly much shorter than the length of the update interval.

Overall, while the maintenance history and propagation situation for this object is not the best, it is good enough to serve as a basis for risk assessment, presuming that other issues (e.g., space weather) do not ultimately jeopardize the credibility of the propagation.

Q.3 Primary and Secondary Object Trajectories

The ground trace plot shown in Figure Q-1 depicts the two satellite trajectories in relation to each other and identifies the geographical position of their point of closest approach.

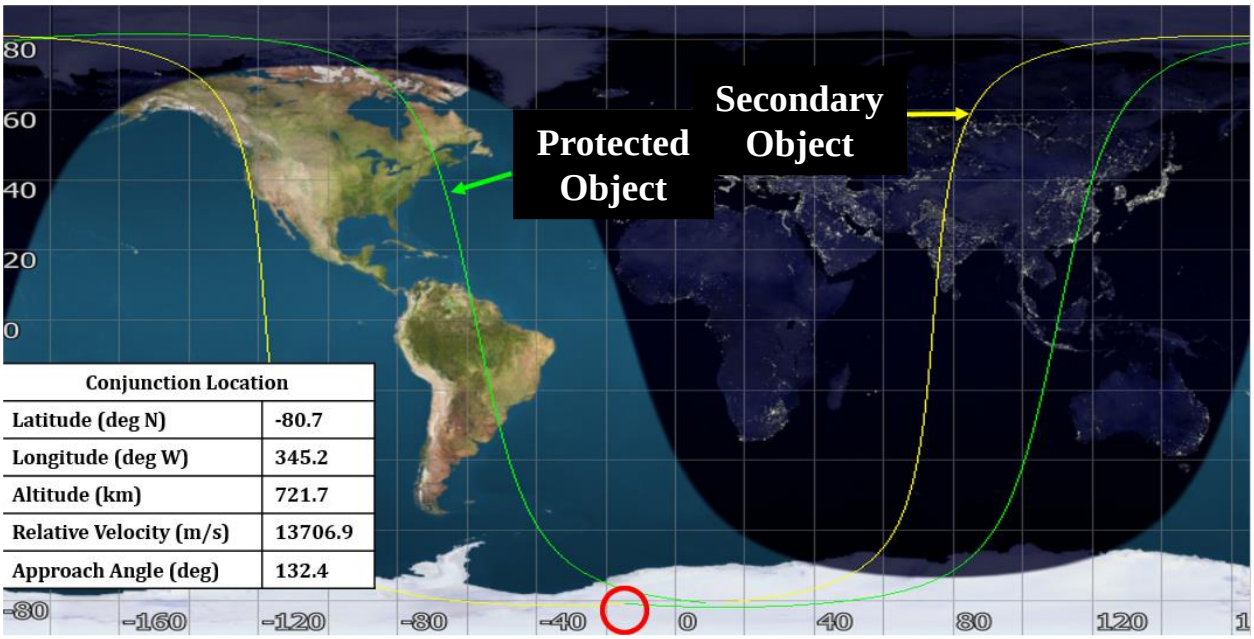

Conjunction Location	
Latitude (deg N)	-80.7
Longitude (deg W)	345.2
Altitude (km)	721.7
Relative Velocity (m/s)	13706.9
Approach Angle (deg)	132.4

Figure Q-1 Ground Trace Plot

In the above encounter, the closest-approach point—over Antarctica—is far away from the field of regard of any of the SSN ground sensors, meaning that this part of both satellites' trajectories will not be modeled as well as if the ground sensor were directly under the point of closest approach. The relative velocity value indicated in Figure Q-1, almost 14 km/sec, is both very fast and typical for LEO conjunctions; it is certainly large enough to allow hyperkinetic assumptions about the conjunction to inhere and thus to allow the use of simplified approaches to calculating the probability of collision, such as the 2D Pc.

The approach angle may also be of some interest. A zero-degree approach angle describes a situation in which one object "chases" another, usually presenting lower-velocity encounters; a 180-degree approach angle constitutes a "head-on" collision. In both such instances, in-track error plays a smaller role in the conjunction dynamics because it controls the timing of any collision more than whether a collision would in fact take place. (This is of course only partially true because in-track error is usually correlated with radial error and thus will engender a radial component.) Values in between these extremes describe the typically encountered oblique situation, which is the case in this particular event being evaluated.

Q.4 Conjunction Plane Information

The Figure Q-2 visual, called a Conjunction Plane Plot, communicates certain information about the event. In interpreting this representation, it may be helpful to review the development of the 2D Pc calculation methodology outlined in Appendix N.

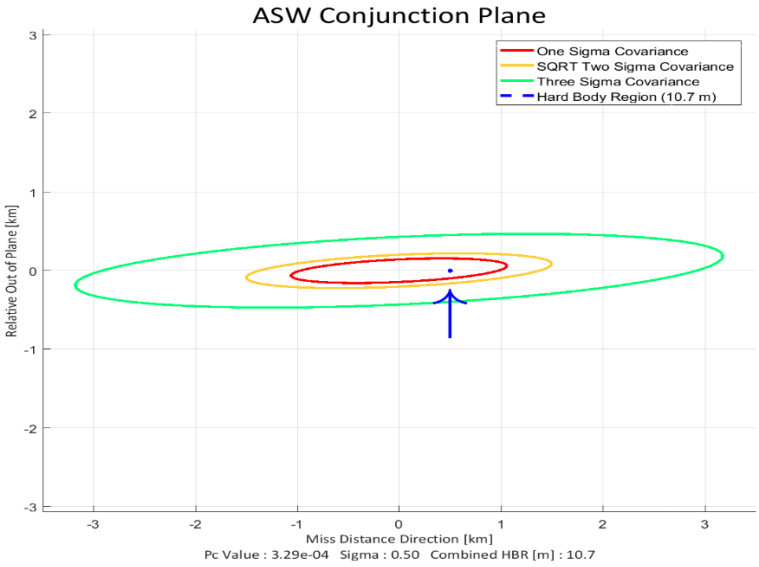

Figure Q-2 Conjunction Plane Plot

The relative miss vector lies along the x-axis, with one end at the origin and the other terminating at the blue dot. This blue "dot" is in fact a circle with a radius equaling the hard-body radius (HBR) that represents the combined sizes of the primary and secondary objects. The ellipses represent the combined uncertainty of the primary and secondary objects' positions, here resolved from an ellipsoid to an ellipse in the plane in which a collision, should it occur, would take place.

For low-likelihood conjunctions, the blue dot is far outside of the three-sigma ellipse, and frequently, the ellipse itself is collapsed onto the x-axis, indicating that the in-track error is dominating the conjunction. In the case being discussed, the situation is different: the blue dot is within the one-sigma error ellipse, and the ellipse itself has visible definition, indicating that the uncertainties in this situation are more varied.

Q.5 Collision Probability Evolution

The Figure Q-3 graphic gives a time history of the probability of collision (Pc) during this event's development.

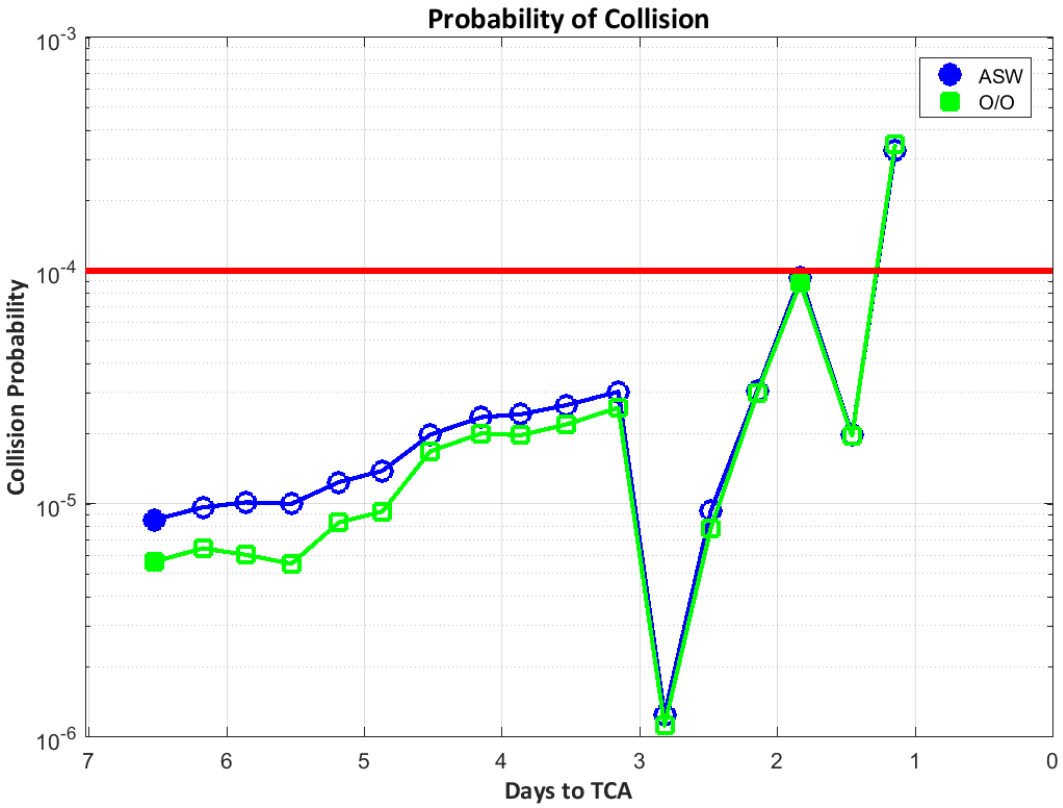

Figure Q-3 Probability of Collision Time-History Plot

While it is true that in most cases operational practice is grounded correctly on the Pc at the "mitigation action commitment point" (namely, that temporal point before TCA at which a decision must be rendered regarding whether a mitigation action will take place), the behavior of the Pc over the event's history does help to indicate whether the event's risk assessment data are stable enough to allow a durable risk assessment decision to be made.

Figure Q-3 shows the Pc time history:

- For the primary and secondary objects' states and covariances based on the skin-tracking results (indicated as "ASW" in the legend), and
- For the primary object's state and covariance derived from a submitted owner/operator ephemeris (indicated as "O/O" in the legend).

An additional feature of Figure Q-3 is that the graphic markers (square or circle) are filled in for the particular updates that received new tracking.

Figure Q-3 makes clear that the secondary object is not particularly well tracked; most of the updates, noted by the open markers, are based only on the update of the space weather coefficients and do not constitute a new state estimate resulting from fresh tracking. However, the significant state update that does contain new tracking (just a little less than two days to TCA) is barely under the mitigation threshold (red line), and after additional space weather

updates, the last such update before the mitigation action commitment point (one day) exceeds the red threshold. While there is a large variation observed in the Pc history, it is not so extreme as to indicate to an analyst that the situation is so unstable that a mitigation action cannot be planned or counselled wisely. As such, based (provisionally) on Figure Q-3, it would be recommended for this O/O to take a mitigation action.

Q.6 Miss Distance Evolution

While the Pc is the collision likelihood metric of choice, it is helpful to examine the miss distance history as well to see if it is manifesting a dramatically different pattern from the Pc history.

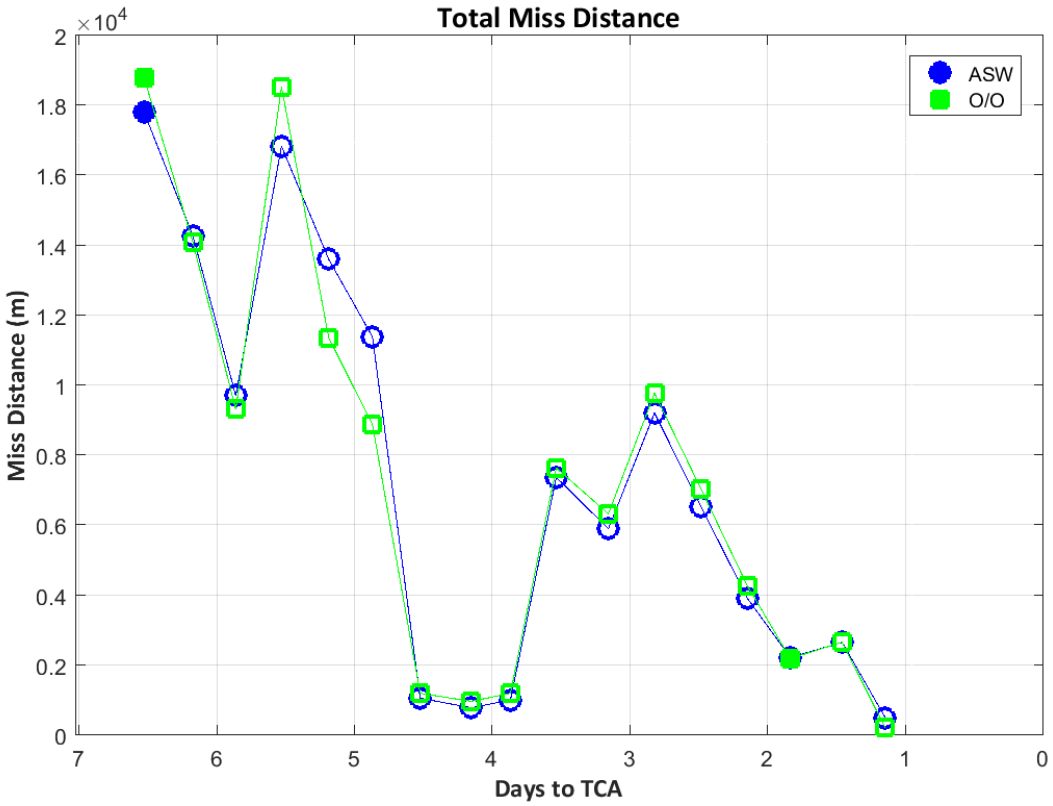

Figure Q-4 Total Miss Distance Plot

Miss distance is one of the principal inputs to the Pc, but the combined covariance and HBR are also important. There are cases in which the miss distance behaves in a manner that would seem to reduce collision risk but the covariance evolution is such that the collision likelihood remains high; in such situations, further investigation is prudent.

When comparing Figure Q-4 to the Pc history, one observes a situation in which the miss distance evolution is not in obvious lock-step with the Pc evolution, which is not an unusual outcome given what appears to be happening with the covariance evolution at the same time. But one also observes a situation for which the miss distance has moved to a very low value in the

last update. Even though this is not brought about via a tracking update but just space weather model updates, it is small enough to have driven the Pc above the mitigation threshold. While in principle it could change at the next update and push the Pc below the threshold, the situation is not so contradictory that one would assert that it has no predictive force.

As such, the miss distance behavior does not work against a conclusion that collision mitigation is appropriate.

Q.6.1 Miss Distance Component Behavior

In Figure Q-5, the individual miss distance components are examined, which is a more meaningful display of the time history of this particular datum.

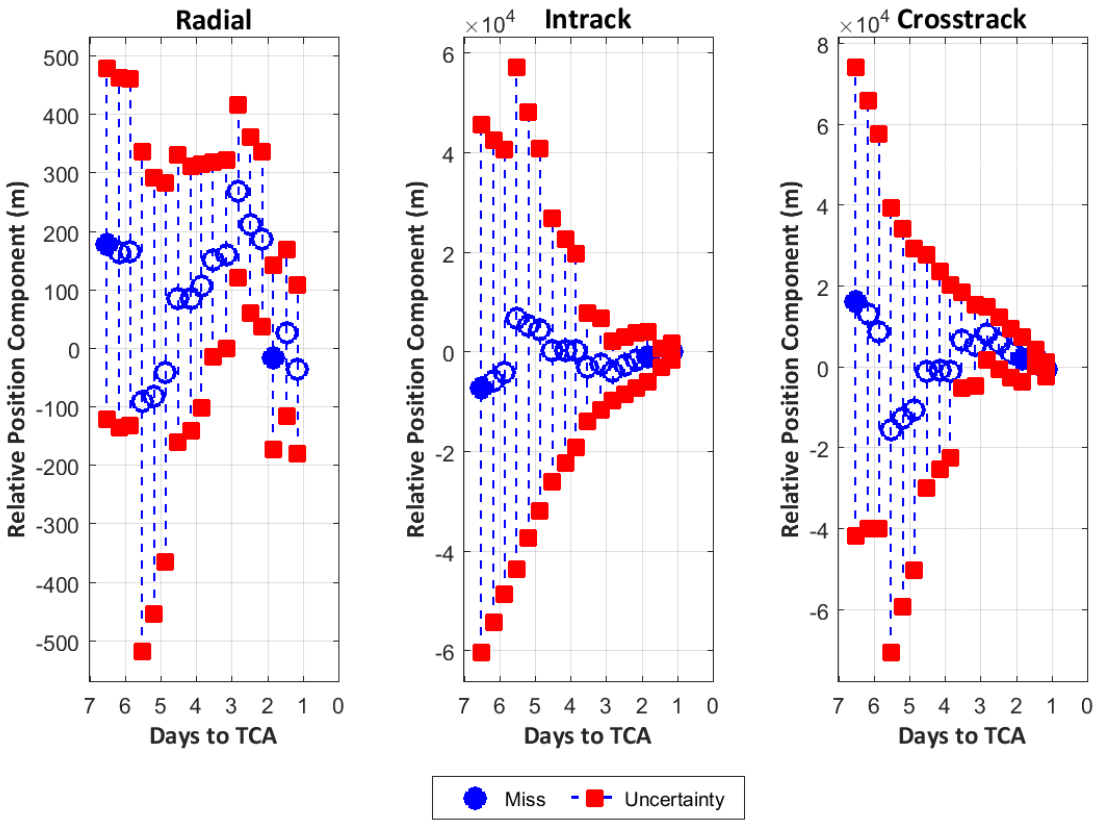

Figure Q-5 Componentized Miss Distance Plot

Figure Q-5 also gives a time-history of miss distance behavior, but it separates the miss distance, helpfully, into three components centered on the primary object:

- The radial miss (in the direction toward the center of the Earth),
- The in-track miss (perpendicular to the radial miss in the plane of the orbit), and
- The cross-track miss (the direction perpendicular to this plane).

The blue circles represent the signed miss distance in the particular component of interest (and if filled in, tracking was received as part of the state estimate update that produced that miss distance), and the red squares represent the one-sigma uncertainty for that miss component.

Ideal behavior is a set of blue circles that essentially stay at the same value update to update, while the red squares shrink closer to that value as the propagation length is decreased from 7 days to ~1 day.

The in-track results above (middle graph) essentially exhibit this behavior: the in-track miss does not fluctuate wildly (although the y-axis scale should be kept in mind), and the uncertainties shrink nicely as the event develops.

The situation is somewhat less well-behaved for the cross-track graph (far right), but in the main, the actual miss does converge to a value while the uncertainties shrink.

The radial component, however, does not behave so nicely; and since this miss component is the most determinative for the Pc, it needs to be watched carefully.

- First, one should notice how much smaller the radial miss values are compared to the other two components. It is because of this small radial miss that this event is a high-risk event in the first place.
- Second, its evolution would have to be characterized as at least somewhat unstable: it changes sign and does not uniformly focus on a single value over time. However, such behavior is not truly unusual for the radial component.
- Third, when fresh tracking is finally obtained, the miss distance does jump and changes sign, but it jumps to a worrisome value (nearly zero) and does not stray far from that value as the event pushes forward to the mitigation action commitment point.

The fact that this key component of the high-risk designation stays reasonably stable coming into the mitigation action commitment point gives additional confidence that the reasonably high Pc value should be taken seriously.

Q.6.2 Normalized Component Miss Distance Value Comparison

Figure Q-6 is a different way to render the development of the componentized miss distance as the event builds to TCA. Rather than actual component miss distance values, Figure Q-6 represents normalized values: the change in componentized miss distance divided by the expected error in that component from the previous update. In essence, Figure Q-6 reflects how well or poorly each update behaves with regard to its expected error.

Ideal performance would be for updates to sit very close to the zero line: there would be strong agreement update to update, and any actual difference between predictions would be small compared to the prediction error or, to be more precise, ~68% of such ratios would fall within the +1 to -1 regions.

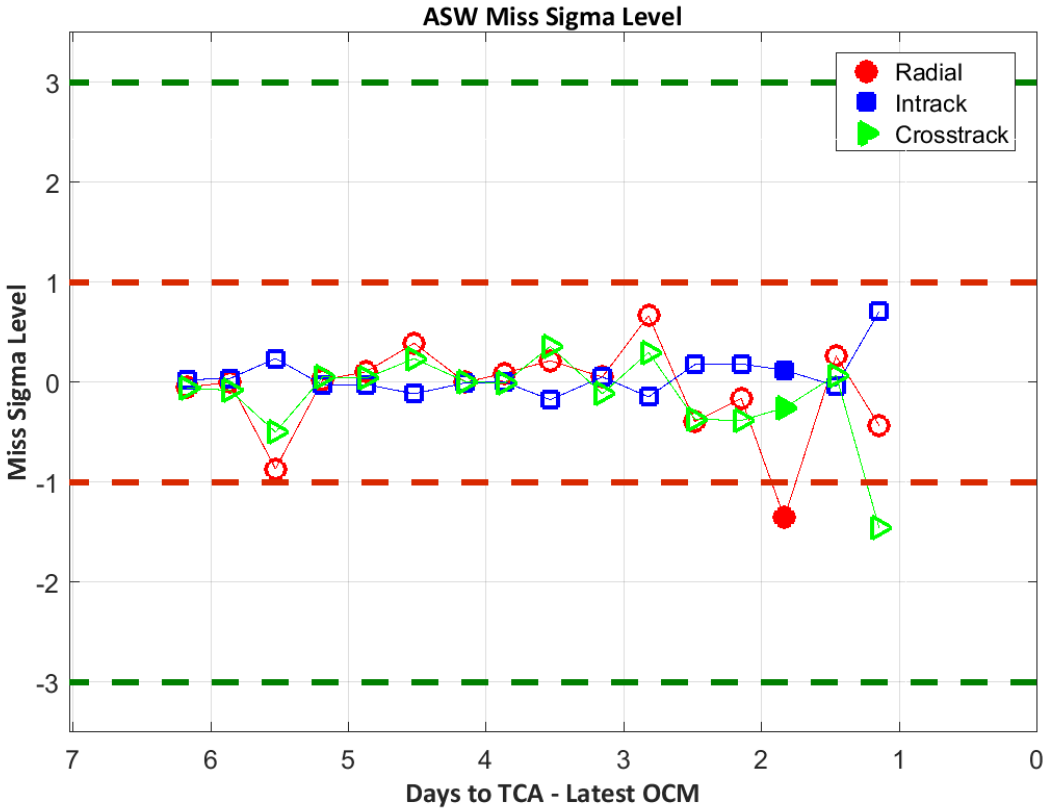

Figure Q-6 State Comparison Consistency Plot

The behavior shown in Figure Q-6 is quite desirable. Most values are very near the zero-line, and the few that are not do not deviate much beyond the one-sigma region. One can encounter situations in which gyrations beyond the three-sigma region occur throughout; in comparison to that, the above is very well behaved. It is also not unusual to see notable changes introduced as the result of additional tracking; the value for the radial component right after the two-days-to-TCA vertical line (red filled dot) is an example of this.

Overall, this is a reasonably well-behaved event whose final result can be trusted to yield an actionable result.

Q.7 Space Weather Considerations

The space weather situation is important to consider when ascertaining whether the orbital dynamics are expected to be sufficiently stable that the data examined at the mitigation action commitment point are expected to inhere until TCA.

Q.7.1 Solar Storms

The main area of interest in Figure Q-7 is the expectation of effects from solar storms such as coronal mass ejections (CMEs), and these are best predicted by examining the disturbance storm time (Dst) parameter prediction.

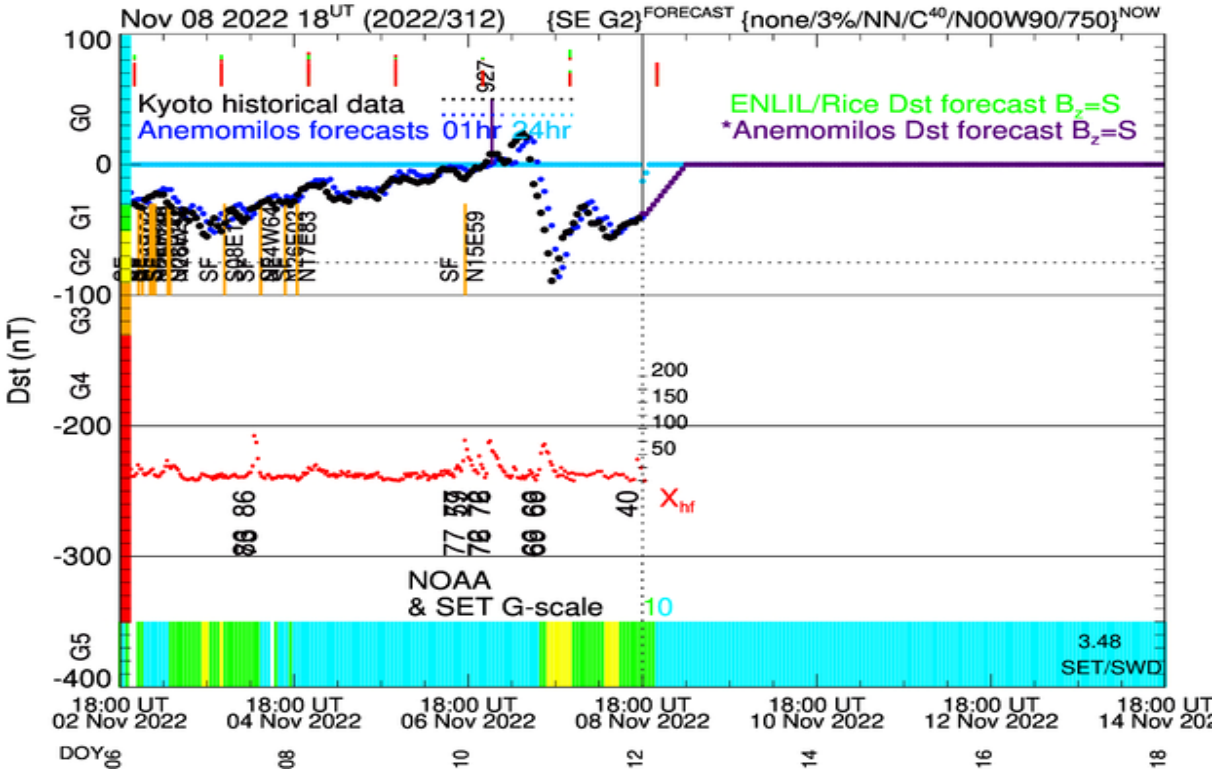

(*Image from* http://sol.spacenvironment.net/~sam_ops/current_data/Dst_streamB_forecast.jpg)

Figure Q-7 Solar Storm Prediction

The upper part of Figure Q-7 gives both a history and prediction of this parameter: the historical data are in black, the one-hour Anemomilos (the model used by the DOD to predict this parameter) given in blue, and the longer-term Anemomilos forecasts given in purple; the current time is indicated by the vertical dotted line.

Dips in Dst are the behavior of significance with a threshold of -75 nanoTeslas being the threshold used by CARA to indicate a disturbed situation. In Figure Q-7, one can observe a dip below this value, then a "recovery" increase, then some residual dipping before steadying off and heading to the zero value. The prediction shows a linear increase to the zero value, which indicates a stable situation.

The takeaway from Figure Q-7 is that, while the space weather situation was somewhat perturbed in the event's recent history, at the current time (indicated by the vertical dotted line), it appears to have largely stabilized, and the future situation looks to be only more stable.

Therefore, one can be reasonably comfortable acting on the present data at the maneuver commitment point since space weather is not likely to cause unexpected changes in drag predictions through the time of closest approach.

Q.7.2 Space Weather Modeling

Figure Q-8 communicates the expected effect on the probability of collision if the space weather situation has been mismodeled in the predicted object trajectories.

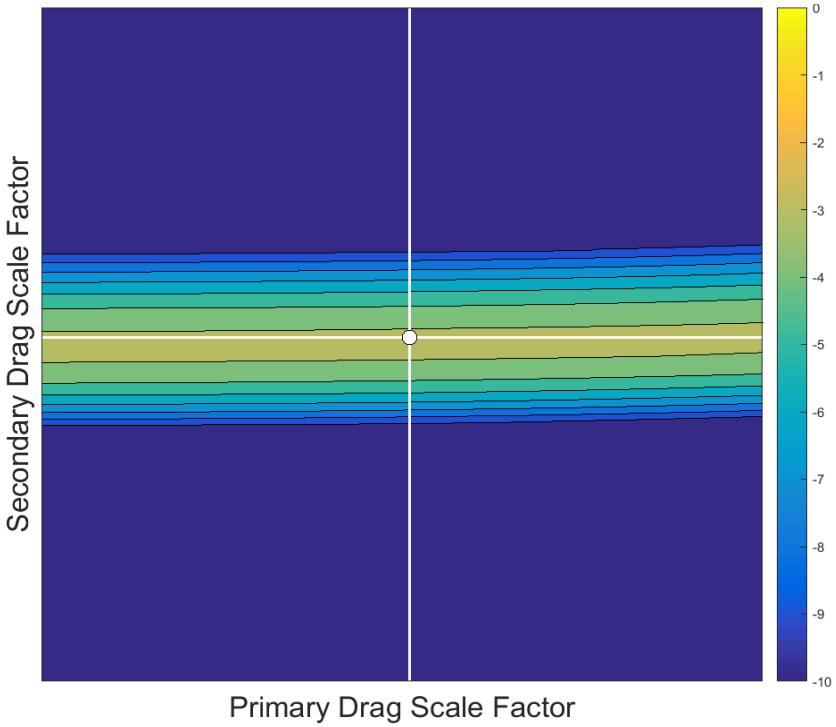

Figure Q-8 Space Weather Trade-Space Plot

Note that Figure Q-7 and the outcome of this particular event outline a situation in which Figure Q-8 probably would not be used operationally, but in a discussion of this type, it seems appropriate to include the information nonetheless.

To determine whether space weather has been mismodeled, one first recognizes that, in the drag equation, the atmospheric density estimate and the ballistic coefficient are multiplicatively coupled; this means that the effect of changing one of these parameters can be emulated by changing the other. To produce Figure Q-8, the ballistic coefficients for the primary and secondary objects were increased and decreased incrementally by up to half an order of magnitude in each direction (e.g., the "Primary Drag Scale Factor" on the x-axis spans from -0.5 to 0.5 in log space). This produces the same effect on predicted position if the atmospheric density were mismodeled by that amount. The colors on the intensity plot are the base-ten logarithm of the Pc.

What is important in the presentation, however, is not the actual Pc values but the morphology of the plot. If the midpoint (which represents the current actual solution) is on a "ridge," as in Figure Q-8, any mismodeling of the atmospheric density will result in a lower Pc value. Thus, if the current Pc is below one's threshold for action, one can embrace a decision to dismiss the

conjunction; i.e., if the current Pc value is below the threshold, and any mismodeling is expected only to lower the Pc from that value, then the event can be considered safe.

A presentation that is essentially one-color results in a similar conclusion because in such a case, the presentation is indicating that the event is simply not sensitive to atmospheric density mismodeling. If, however, the midpoint dot is on a "slope" (e.g., if it were on one of the light blue lines in Figure Q-8), then mismodeling could potentially either increase or decrease the Pc.

Thus, in such a case, the event is sensitive to atmospheric density mismodeling, and changes may be observed in future orbit determination updates in either direction that could affect the decision to maneuver. If the event is close to the red threshold, CARA would typically recommend maneuvering despite the space weather uncertainty for conservatism.

Q.8 Mitigation Maneuver Planning

To assist O/Os in planning mitigation actions, a "Maneuver Trade-Space" plot similar to Figure Q-9 is produced.

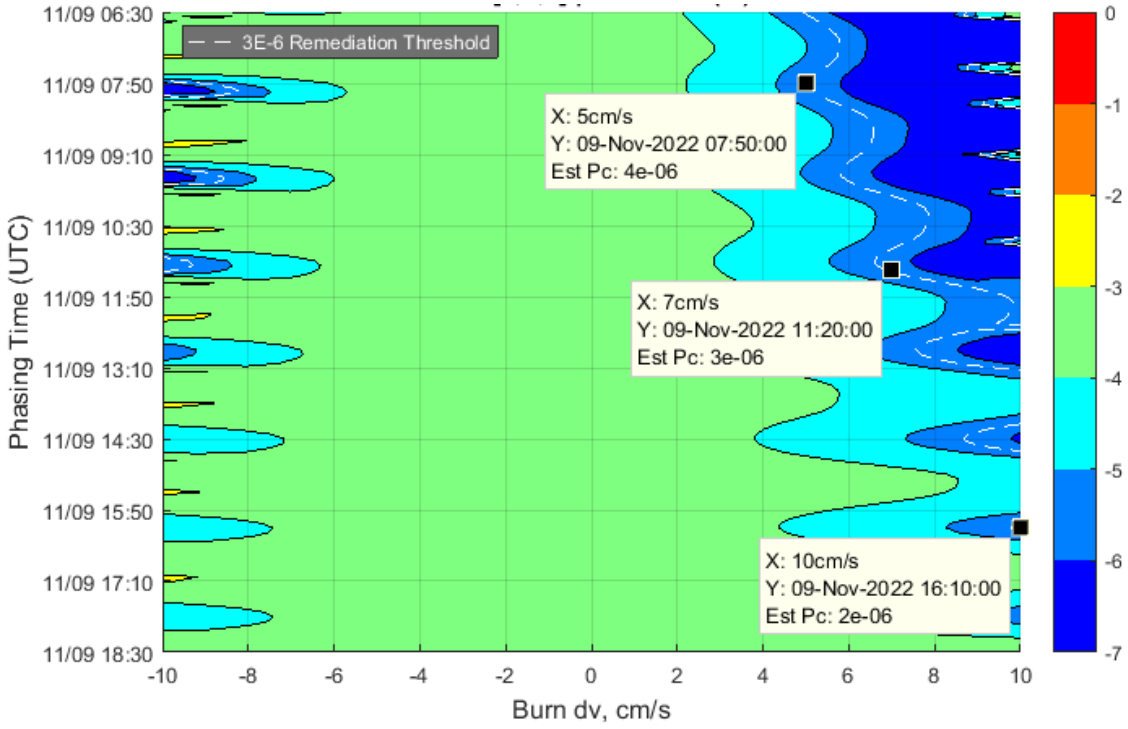

Figure Q-9 Maneuver Trade-Space Plot

A potential mitigation burn, taken from a variety of different burn sizes at a variety of different execution times, is placed into the primary object's ephemeris, the altered ephemeris is propagated forward, new Pcs for both the main conjunction under consideration and any other conjunctions that arise from this altered trajectory are calculated, and the Pc that is an amalgamation of these individual Pc values is calculated. This calculation is run over and over, working through the entire range of burn intensities and burn times, and from the results, an

intensity plot like Figure Q-9 is constructed. The colors indicated on the second y-axis at right indicate the Pc (1E-X, where X is the value on the axis) that will be achieved if a burn of the magnitude chosen on the x axis and the phasing time chosen on the right axis is executed. Choosing a maneuver time and magnitude that result in a Pc of 1E-07 (dark blue) would be considered to fully mitigate the conjunction risk.

A number of interesting conclusions can be drawn from a Maneuver Trade-Space plot. If it is the case that the O/O wishes to mitigate the risk down to the CARA-recommended level of 3E-06, then a maneuver should be chosen that lies along the dashed white line above. The longer one waits to perform the maneuver, the larger the maneuver will need to be; the maneuver possibility shown in the bottom right of the graph is twice as large as the one shown at the top right, so maneuvering early allows a smaller maneuver to fully mitigate the conjunction. However, it is also often the case that waiting an additional half-day will allow more tracking data to be collected that will shrink the covariance and potentially push the Pc below the red threshold, meaning no maneuver would be necessary at all. This tension ultimately must be resolved by the O/O: does the O/O want to commit early and lock in a smaller maneuver, or does the O/O want to wait to act until the maneuver commitment point, hoping that the need for the maneuver will evaporate completely? The risk of waiting is that a large maneuver would be required to mitigate the conjunction, or that it may not be possible to fully mitigate the risk given the size maneuver that the spacecraft has the capability to perform.

Note that Figure Q-9 does not dictate any specific action to the O/O; instead, it provides general guidance for the sizes and timing of maneuvers that that meet chosen mitigation requirements. Based on these data, the O/O selects a promising maneuver (or set of maneuvers), builds them into predicted ephemerides, and submits them to the conjunction assessment screening authority for screening. This latter action is necessary because it is the only way to give assurance of both the safety of the proposed is necessary because it is the only way to give assurance of both the safety of the proposed maneuver (or set of maneuvers) relative to other on-orbit objects and the actual amount of risk reduction that the maneuver (or set of maneuvers) can be expected to yield.

In this example, the collision likelihood is above the CARA mitigation threshold (1E-04) at the maneuver commitment point used by the O/O for this spacecraft, and mitigation actions that appropriately reduce the risk are available and not large enough to negatively affect the satellite's main mission appreciably. Therefore, the O/O made the straightforward decision to perform a mitigation action.